Image reconstruction through metamorphosis

Ozan Öktem, Barbara Gris, Chong Chen

Image reconstruction through metamorphosis

Barbara Gris (bgris.maths@gmail.com)*

Chong Chen (chench@lsec.cc.ac.cn) †

Ozan Öktem (ozan@kth.se) ‡

Abstract

The paper describes a method for reconstructing an image from noisy and indirect observations by registering, via metamorphosis, a template. The image registration part consists of two components, one is a geometric deformation that moves intensities without changing them and the other that changes intensity values. Unlike a registration with only geometrical deformation, this framework gives good results also when intensities of the template are poorly chosen. It also allows for appearance of a new structure. The approach is applicable to general inverse problems in imaging and we prove existence, stability and convergence, which implies that the method is a well-defined regularisation method. We also present several numerical examples from tomography.

Keywords: Inverse problem; indirect registration; metamorphosis.

1 Introduction

A key difficulty in *shape based* and/or *spatiotemporal* image reconstruction is to match an image against an indirectly observed target (*indirect image registration*). In the following, we give a brief overview of these notions along with a short survey of existing results.

Shape based reconstruction The goal in shape based reconstruction is to recover shapes (morphologies) of interior sub-structures of an object whereas variations within these is of less importance. Such imaging studies arise in nano-characterisation of a specimen by means of electron microscopy

*LJLL - Laboratoire Jacques-Louis Lions, UPMC, Paris, France.

†LSEC, ICMSEC, Academy of Mathematics and Systems Science, Chinese Academy of Sciences, Beijing 100190, People's Republic of China

‡Department of Mathematics, KTH – Royal Institute of Technology, Stockholm, Sweden.

[5] or quantification of sub-resolution porosity in materials by means of x-ray phase contrast imaging.

In these imaging applications it makes sense to account for qualitative prior shape information during the reconstruction. Enforcing an exact spatial match between a template and the reconstruction is often unrealistic since shape information is almost always approximate, so the natural approach is to perform reconstruction assuming the structures are 'shape wise similar'.

Spatiotemporal imaging Here one images an object that changes over time, i.e., one needs to recover both the object structure and its time variation from noisy time series of indirect observations (measured data). An important case is when the object is the only entity that varies with time.

Spatiotemporal imaging arises when imaging moving organs in medicine. For more details on this problem, the reader is referred to [10] and the references therein. It is in particular relevant for techniques like positron emission tomography (PET) and single photon emission computed tomography (SPECT) that are used to image the distribution of injected radiopharmaceuticals (activity map). The latter is an inherently dynamic quantity since anatomical structures, like the heart and lungs, undergo motion during the data acquisition, see [35] for a survey of organ motion models. Disregarding organ motion is known to degrade the spatial localisation of the radiotracer, leading to spatially blurred images. To exemplify the above mentioned issues, consider SPECT based cardiac perfusion studies and $_{18}$F-FDG-PET imaging of lung nodules/tumours. The former needs to account for the beating heart and the latter for respiratory motion of the lungs and thoracic wall. Studies show a maximal displacement of 23 mm (average 15–20 mm) due to respiratory motion [31] and 42 mm (average 8–23 mm) due to cardiac motion in thoracic PET [37]. Finally, even when organ motion can be neglected, there are other dynamic processes, such as the uptake and wash-out of radiotracers from body organs. Visualising such kinetics of the radiotracers can actually be a goal in itself as is the case in dynamic PET, which is commonly used in pre-clinical imaging studies related to drug discovery/development [20].

Indirect image registration (matching) The aim in image registration is to deform a template image so that it matches a target image. This becomes challenging when the template is allowed to undergo non-rigid deformations.

Diffeomorphic image registration is a well developed framework that meets this purpose. Here, the image registration problem is recast as the problem of finding a suitable diffeomorphism that deforms the template by a group action into the target image [40, 2]. The underlying assumption is

that the target image is contained in the orbit of the template under the group action of diffeomorphisms. This can be stated in a very general setting where diffeomorphisms act on various deformable objects, like landmark points, curves, surfaces, scalar images, or even vector/tensor valued images.

The registration problem becomes even more challenging in *indirect image registration*, which is the case when the target is only known indirectly through measured data. Application of small diffeomorphic deformations in the context of indirect image registration is presented in [29]. One can in a similar manner use large deformation diffeomorphic metric mapping (LDDMM) framework in indirect image registration as shown in [21, 11].

2 Overview of paper and specific contributions

The paper adapts the metamorphosis framework [36] to the indirect setting. Metamorphosis extends the LDDMM framework (diffeomorphometry) [40, 25] by allowing diffeomorphic changes to *both* the geometry of the template and its grey-scale values (intensities). As detailed below, an important feature of metamorphosis compared to diffeomorphometry is its capability to reconstruct images even when the template has erroneous grey-scale values that lack geometric features, e.g., in the form of a noisy background. We also show how indirect registration by metamorphosis formally defines a regularisation method for inverse problems in imaging, satisfying properties of existence, stability and convergence. Next, we study robustness with respect to choice of regularisation parameters. Finally, we provide an algorithm and its implementation[1] that relies on a Fourier transforms for kernel convolutions and a Euler integration scheme for the temporal integration. Note that other approaches could be developed, like [28] where the time discrete path method in [15] is extended to the indirect setting, or adaptation of the robust schemes for diffeomorphic registration developed in [22, 23].

We start by recalling necessary theory from LDDMM-based indirect registration (section 3). Using these notions, we next adapt the metamorphosis framework to the indirect setting (section 4) and present our proof that this is a regularisation method (section 4.3). Its numerical implementation is outlined in section 4.4. Finally, we present several numerical examples from indirect registration in 2D tomography (section 5). In particular, we give a preliminary result for motion reconstruction when the acquisition is done at multiple time points. We also study the robustness of our methods w.r.t. the choice of regularisation parameters.

[1] https://github.com/bgris/IndirectMatchingMetamorphosis

3 Indirect diffeomorphic registration

3.1 Large diffeomorphic deformations

Following [1], (large) diffeomorphic deformations are defined by flows of time-varying vector fields. More precisely, let $\Omega \subset \mathbb{R}^d$ be a fixed bounded domain and let $X := L^2(\Omega, \mathbb{R})$ represent grey scale images on Ω. Next, let V denote a fixed Hilbert space of vector fields on $\mathbb{R}^d$. We will assume $V \subset C_0^p(\Omega)$, i.e., the vector fields are supported on Ω and p times continuously differentiable. Finally, $L^1([0,1], V)$ denotes the space of time-dependent V-vector fields that are integrable, i.e.,

$$\boldsymbol{\nu}(t, \,\cdot\,) \in V \quad \text{and} \quad t \mapsto \big\|\boldsymbol{\nu}(t, \,\cdot\,)\big\|_{C^p} \text{ is integrable on } [0,1].$$

The following (semi) norm on $L^1([0,1], V)$ will be frequently used:

$$\|\boldsymbol{\nu}\|_p := \Big(\int_0^1 \big\|\boldsymbol{\nu}(t, \,\cdot\,)\big\|_V^p \,\mathrm{d}t\Big)^{1/p}.$$

Here, $\|\,\cdot\,\|_V$ is the norm on the Hilbert space V of vector fields that is given by the inner product.

The following proposition shows that velocity fileds in $L^1([0,1], V)$ can be used to generate flows in $\mathrm{Diff}_0^p(\Omega)$ (set of p-diffeomorphisms that are supported in $\Omega \subset \mathbb{R}^d$, and if Ω is unbounded, tend to zero towards infinity). This yields a method for generating diffeomorphisms.

Proposition 1. *Let $\boldsymbol{\nu} \in L^1([0,1], V)$ and consider the ordinary differential equation (flow equation):*

$$\begin{cases} \dfrac{\mathrm{d}}{\mathrm{d}t}\phi(t,x) = \boldsymbol{\nu}\big(t, \phi(t,x)\big) \\ \phi(0,x) = x \end{cases} \qquad \text{for any } x \in \Omega \text{ and } t \in [0,1]. \tag{1}$$

Then, (1) has a unique absolutely continuous solution $\phi(t, \,\cdot\,) \in \mathrm{Diff}_0^p(\mathbb{R}^d)$.

The above result is proved in [1] and the unique solution of (1) is henceforth called the *flow of* $\boldsymbol{\nu}$. We henceforth use the notation $\varphi_{s,t}^{\boldsymbol{\nu}} \colon \mathbb{R}^d \to \mathbb{R}^d$, which refers to

$$\varphi_{s,t}^{\boldsymbol{\nu}} := \phi(t, \,\cdot\,) \circ \phi(s, \,\cdot\,)^{-1} \quad \text{for } s,t \in [0,1] \tag{2}$$

where $\phi \colon \Omega \to \mathbb{R}^d$ denotes the unique solution to (1).

As stated next, the set of diffeomorphisms that are given by solving the flow equation (1) forms a group that is a complete metric space [1]. Its elements are called *large diffeomorphic deformations*.

Proposition 2. *Let $V \subset C_0^p(\Omega)$ $(p \geq 1)$ be an admissible reproducing kernel Hilbert space (RKHS) and define*

$$G_V := \Big\{ \phi \colon \mathbb{R}^d \to \mathbb{R}^d \mid \phi = \varphi_{0,1}^{\boldsymbol{\nu}} \text{ for some } \boldsymbol{\nu} \in L^2\left([0,1], V\right) \Big\}. \tag{3}$$

Then G_V forms a sub-group of $\mathrm{Diff}_0^p(\mathbb{R}^d)$ that is a complete metric space under the metric

$$\begin{aligned} \mathrm{d_G}(\phi_1, \phi_2) &:= \inf \Big\{ \|\boldsymbol{\nu}\|_1 : \boldsymbol{\nu} \in L^1([0,1], V) \text{ and } \phi_1 = \phi_2 \circ \varphi_{0,1}^{\boldsymbol{\nu}} \Big\} \\ &= \inf \Big\{ \|\boldsymbol{\nu}\|_2 : \boldsymbol{\nu} \in L^1([0,1], V) \text{ and } \phi_1 = \phi_2 \circ \varphi_{0,1}^{\boldsymbol{\nu}} \Big\}. \end{aligned}$$

The group G_V may act on X through the *geometric group action*, which defines a deformation operator

$$\mathcal{W} \colon G_V \times X \to X \quad \text{where} \quad \mathcal{W}(\phi, I_0) := I_0 \circ \phi^{-1}. \tag{4}$$

We conclude by characterizing the regularity properties of flows of velocity fields as well as the group action in (4), the proof is given in [7]. These results will play an important role in what is to follow.

Proposition 3. *Assume $V \subset C_0^p(\Omega)$ $(p \geq 1)$ is a fixed admissible Hilbert space of vector fields on Ω and $\{\boldsymbol{\nu}^n\}_n \subset L^2\left([0,1], V\right)$ a sequence that converges weakly to $\boldsymbol{\nu} \in L^2\left([0,1], V\right)$. Then, the following holds with $\varphi_t^n := \varphi_{0,t}^{\boldsymbol{\nu}^n}$:*

1. *$(\varphi_t^n)^{-1}$ converges to $(\varphi_{0,t}^{\boldsymbol{\nu}})^{-1}$ uniformly w.r.t. $t \in [0,1]$ and uniformly on compact subsets of $\Omega \subset \mathbb{R}^d$.*
2. *$\lim_{n \to \infty} \left\| \mathcal{W}(\varphi_t^n, I_0) - \mathcal{W}(\varphi_{0,t}^{\boldsymbol{\nu}}, I_0) \right\|_X = 0$ for any $I_0 \in X$.*

3.2 Indirect image registration

Image registration (matching) is the task of deforming a given template image $I_0 \in X$ so that it matches a given target image $I^* \in X$ [6, 41].

The above task can also be stated in an *indirect* setting, which refers to the case when the template $I_0 \in X$ is to be registered against a target $I^* \in X$ that is only indirectly known through data $g \in Y$ where

$$g = \mathcal{A}(I^*) + e. \tag{5}$$

In the above, $\mathcal{A} \colon X \to Y$ (forward operator) is known and assumed to be differentiable and $e \in Y$ is a single sample of a Y-valued random element that denotes the measurement noise in the data.

Access to a shape prior (template), as in indirect registration, can have profound effect in solving challenging inverse problem in imaging. As shown in [11], tomographic imaging problems that are otherwise intractable (highly

noisy and sparsely sampled data) can be successfully addressed using indirect registration even when the template has a shape that is far from the true unknown target image that gave rise to measured data. The next step is to specify what is meant by *deforming a template image* and we consider diffeomorphic (non-rigid) deformations, i.e., diffeomorphisms that deform images by acting on them through a group action.

LDDMM-based registration Image registration by large diffeomorphic (non-rigid) deformations is typically formulated as minimising the functional

$$G_V \ni \phi \mapsto \frac{\gamma}{2}\,\mathrm{d_G}(\mathrm{Id},\phi)^2 + \big\|\mathcal{W}(\phi, I_0) - I^*\big\|_X^2 \quad \text{for given } \gamma > 0.$$

If V is admissible, then one can show that minimising the above functional on G_V is equivalent to minimising the following functional on $L^2([0,1],V)$: [40, Theorem 11.2 and Lemma 11.3]:

$$L^2([0,1],V) \ni \boldsymbol{\nu} \mapsto \frac{\gamma}{2}\|\boldsymbol{\nu}\|_2^2 + \big\|\mathcal{W}(\varphi_{0,1}^{\boldsymbol{\nu}}, I_0) - I^*\big\|_X^2 \quad \text{given } \gamma > 0.$$

Such a reformulation is advantageous since $L^2([0,1],V)$ is a vector space, whereas G_V is not. Hence, it is easier to devise algorithms for minimising a functional over $L^2([0,1],V)$ rather than over G_V.

As shown in [11], one can extend the above to the indirect setting where the image target I^* is not observed but only a data target g (*LDDMM-based indirect registration*). We simply need to replace the data fidelity term $\big\|\mathcal{W}(\varphi_{0,1}^{\boldsymbol{\nu}}, I_0) - I^*\big\|_X^2$ with one that is adapted for indirect observations, which will involve the forward operator $\mathcal{A}$ and a data negative log-likelihood $\mathcal{L}\colon Y \times Y \to \mathbb{R}$. More precisely, the corresponding indirect registration problem can be adressed by minimising the functional

$$L^2([0,1],V) \ni \boldsymbol{\nu} \mapsto \frac{\gamma}{2}\|\boldsymbol{\nu}\|_2^2 + \mathcal{L}\big((\mathcal{A}\circ\mathcal{W})(\varphi_{0,t}^{\boldsymbol{\nu}}, I_0), g\big).$$

The functional $\mathcal{L}\colon Y \times Y \to \mathbb{R}$ is typically given by an appropriate affine transform of the data negative log-likelihood [4], in which case minimising $f \mapsto \mathcal{L}\big(\mathcal{A}(f), g\big)$ amounts to seeking a maximum likelihood solution of (5).

An interpretation of the above is that the template image I_0, which is assumed to be given a priori, acts as a *shape prior* when solving the inverse problem in (5) and $\gamma > 0$ is a regularisation parameter that governs the influence of this shape priori against the need to fit measured data. This interpretation becomes more clear when one re-formulates LDDMM-based indirect registration as

$$\begin{cases} \min\limits_{\boldsymbol{\nu}\in L^2([0,1],V)} \left[\dfrac{\gamma}{2}\|\boldsymbol{\nu}\|_2^2 + \mathcal{L}\Big((\mathcal{A}\circ\mathcal{W})\big(\phi(1,\,\cdot\,), I_0\big), g\Big)\right] \\ \dfrac{d}{dt}\phi(t,x) = \boldsymbol{\nu}\big(t,\phi(t,x)\big) \quad (t,x) \in \Omega\times[0,1], \\ \phi(0,x) = x \quad x \in \Omega. \end{cases} \tag{6}$$

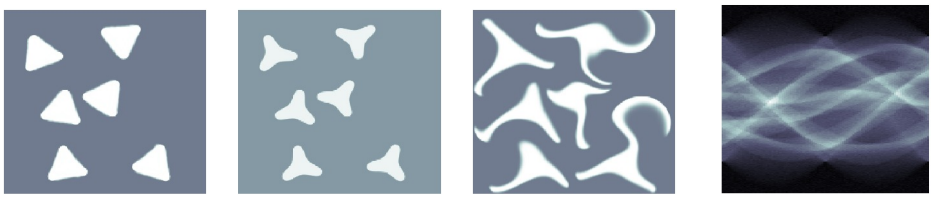

(a) Template. (b) Target. (c) Reconstruction. (d) Data.

Figure 1: Reconstruction (c) by LDDMM-based indirect registration using a template (a) with a geometry that matches the target (b), but with incorrect background intensity values. Target is observed indirectly through tomographic data (d), which is 2D parallel beam Radon transform with 100 evenly distributed directions (see section 5.1 for details). The artefacts in the reconstruction are due to incorrect background intensity in template.

4 Metamorphosis-based indirect registration

4.1 Motivation

The LDDMM-based indirect registration with geometric group action outlined in section 3.2 is remarkably stable when the template has correct topology and intensity levels [11].

Usage of the geometric group action, however, prevents creating or removing intensity, e.g., it is not possible to start out from a template with a single connected structure and deform it to a image with two separated structures. Figure 1 shows the effect that erroneous intensity has on LDDMM-based indirect registration. This severely limits the usefulness of LDDMM-based indirect registration, e.g., spatiotemporal images (movies) are likely to involve changes in both geometry (objects appear or disappear) and intensity.

One approach to address this drawback of LDDMM-based indirect registration is to replace the geometric group action with one that alters intensities, e.g., a mass preserving group action [11]. This allows to correct motion artefacts in PET as shown in [16, 17, 18] but not to model changes in intensities that do not come from a geometric change. Another is to keep the geometric group action, but replace LDDMM with a framework that model the transformation of an image by a combination of a diffeomorphic deformation and intensities changes. The latter leads to metamorphosis-based indirect registration, which we next describe.

4.2 The metamorphosis framework

Just like in LDDMM, diffeomorphisms are generated by flows (1). The difference in metamorphosis is that these diffeomorphisms are combined with

intensities changes. Hence, image registration by LDDMM is restricted to targets that lie in the orbit of the template under the diffeomorphic group action whereas in metamorphosis, the ability to change intensities allows one to reach *any* target in X [36]. As such, metamorphosis extends LDDMM.

To proceed, we start by the abstract definition of metamorphosis.

Definition 1 (Metamorphosis [36])**.** *Let $V \subset C_0^p(\Omega)$ be an admissible Hilbert space, G_V is defined as in (3), and '$\cdot$' denotes some group action of G_V on X. A* metamorphosis *is a curve $t \mapsto (\phi_t, J_t)$ in $G_V \times X$. The curve $t \mapsto f_t := \phi_t.J_t$ is called the* image *part, $t \mapsto \phi_t$ is the* deformation *part, and $t \mapsto f_t$ is the* template *part.*

The image part represents the temporal evolution that is not related to intensity changes (evolution of the underlying geometry), whereas the template part is the evolution of the intensity. Both evolutions, which are combined in metamorphosis, are driven by the *same* underlying flow of diffeomorphisms in G_V.

A important case is when the metamorphosis $t \mapsto (\phi_t, f_t)$ has a deformation part that solves the flow equation (1) and a template part that is C^1 in time. More precisely, let $L^2([0,1], X)$ denote the space of functions in X that are square integrable, i.e.,

$$\zeta(t, \cdot) \in X \quad \text{and} \quad t \mapsto \big\|\zeta(t, \cdot)\big\|_X \in L^2([0,1], \mathbb{R}).$$

A natural norm on $L^2([0,1], X)$ is given by

$$\|\zeta\|_2 := \Big(\int_0^1 \big\|\zeta(t, \cdot)\big\|_X^2 \,\mathrm{d}t\Big)^{1/2}.$$

We will henceforth use the notation

$$L^2([0,1], V \times X) := L^2([0,1], V) \times L^2([0,1], X).$$

Bearing in mind the above notation, for given $(\boldsymbol{\nu}, \zeta) \in L^2([0,1], V \times X)$ and $I_0 \in X$, define the curve $t \mapsto I_t^{\boldsymbol{\nu},\zeta}$ that is absolutely continuous on $[0,1]$ and solves

$$\begin{cases} \dfrac{\mathrm{d}}{\mathrm{d}t} I_t^{\boldsymbol{\nu},\zeta}(x) = \zeta\big(t, \varphi_{0,t}^{\boldsymbol{\nu}}(x)\big) \\ I_0^{\boldsymbol{\nu},\zeta}(x) = I_0(x) \end{cases} \qquad \text{with } \varphi_{0,t}^{\boldsymbol{\nu}} \in G_V \text{ as in (2).} \tag{7}$$

The metamorphosis can now be parametrised as $t \mapsto (\varphi_{0,t}^{\boldsymbol{\nu}}, I_t^{\boldsymbol{\nu},\zeta})$.

Indirect registration The indirect registration problem in section 3.2 can be approached by metamorphosis instead of LDDMM. Similar to LDDMM-based indirect image registration, we define *metamorphosis-based indirect image registration* as the minimization of the objective functional

$$\mathcal{J}_{\gamma,\tau}(\,\cdot\,; g)\colon L^2([0,1], V \times X) \to \mathbb{R}$$

defined as

$$\mathcal{J}_{\gamma,\tau}(\boldsymbol{\nu},\zeta;g) := \frac{\gamma}{2}\|\boldsymbol{\nu}\|_2^2 + \frac{\tau}{2}\|\zeta\|_2^2 + \mathcal{L}\Big(\mathcal{A}\big(\mathcal{W}(\varphi_{0,1}^{\boldsymbol{\nu}}, I_1^{\boldsymbol{\nu},\zeta})\big), g\Big) \tag{8}$$

Here, $I_t^{\boldsymbol{\nu},\zeta}\colon \Omega \to \mathbb{R}$ is given by (7) and we are given fixed regularisation parameters $\gamma, \tau > 0$, measured data $g \in Y$, and initial template $I_0 \in X$ that defines the initial condition $I_0^{\boldsymbol{\nu},\zeta}(x) := I_0(x)$.

Hence, performing metamorphosis-based indirect registration of a template I_0 against a target indirectly observed through data g amounts to solving

$$(\widehat{\boldsymbol{\nu}}, \widehat{\zeta}) \in \operatorname*{arg\,min}_{(\boldsymbol{\nu},\zeta)} \mathcal{J}_{\gamma,\tau}(\boldsymbol{\nu},\zeta;g). \tag{9}$$

As shown in proposition 4, the above optimisation problem has a solution assuming the data discrepancy and the forward operator fulfils some weak requirements. From a solution we obtain the following:

Initial template: $I_0 \in X$ such that $I_0^{\boldsymbol{\nu},\zeta} := I_0$.

Reconstruction: Final registered template $f_1^{\widehat{\boldsymbol{\nu}},\widehat{\zeta}} = \mathcal{W}\big(\varphi_{0,1}^{\widehat{\boldsymbol{\nu}}}, I_1^{\widehat{\boldsymbol{\nu}},\widehat{\zeta}}\big) \in X$.

Image trajectory: The evolution of both geometry and intensity of the template, given by $t \mapsto \mathcal{W}\big(\varphi_{0,t}^{\widehat{\boldsymbol{\nu}}}, I_t^{\widehat{\boldsymbol{\nu}},\widehat{\zeta}}\big)$.

Template trajectory: The evolution of intensities of the template, i.e., the part that does not include evolution of geometry: $t \mapsto I_t^{\widehat{\boldsymbol{\nu}},\widehat{\zeta}}$.

Deformation trajectory: The geometric evolution of the template, i.e., the part that does not include evolution of intensity: $t \mapsto \mathcal{W}(\varphi_{0,t}^{\widehat{\boldsymbol{\nu}}}, I_0)$.

4.3 Regularising properties

In what follows, $X := L^2(\Omega, \mathbb{R})$ and Y a Hilbert space. We will here prove several properties (existence, stability and convergence) of metamorphosis-based indirect image registration. Taken together, these show that metamorphosis-based indirect image registration is a *well defined regularisation method* in the sense of [19].

Proposition 4 (Existence)**.** *Assume $\mathcal{A}\colon X \to Y$ is continuous and the data discrepancy $\mathcal{L}(\,\cdot\,, g)\colon Y \to \mathbb{R}$ is weakly lower semi-continuous for any $g \in Y$. Then, $\mathcal{J}_{\gamma,\tau}(\,\cdot\,, g)\colon L^2([0,1], V \times X) \to \mathbb{R}$ defined through (8) has a minimiser in $L^2([0,1], V \times X)$ for any $I_0 \in L^2(\Omega, \mathbb{R})$.*

Proof. We follow here the strategy to prove existence of minimal trajectories for metamorphosis (as in [9] for instance). One considers a minimising sequence of $\mathcal{J}_{\gamma,\tau}(\,\cdot\,; g)$, i.e., a sequence that converges to the infimum of $\mathcal{J}_{\gamma,\tau}(\,\cdot\,; g)$ (such a sequence always exists). The idea is to prove that

such a minimising sequence has a sub-sequence that converges to a point in $L^2([0,1], V \times X)$, i.e., the infimum is contained in $L^2([0,1], V \times X)$ which proves existence of a minima.

Bearing in mind the above, we start by considering a minimising sequence $\{(\boldsymbol{\nu}^n, \zeta^n)\}_n \subset L^2([0,1], V \times X)$ to $\mathcal{J}_{\gamma,\tau}(\,\cdot\,; g)$, i.e.,

$$\lim_{n\to\infty} \mathcal{J}_{\gamma,\tau}(\boldsymbol{\nu}^n, \zeta^n; g) = \inf_{\boldsymbol{\nu},\zeta} \mathcal{J}_{\gamma,\tau}(\boldsymbol{\nu}, \zeta; g).$$

Since $\{\boldsymbol{\nu}^n\}_n \subset L^2([0,1], V)$ is bounded, it has a sub-sequence that converges to an element $\boldsymbol{\nu}^\infty \in L^2([0,1], V)$. Likewise, $\{\zeta^n\}_n \subset L^2([0,1], X)$ has a sub-sequence that converges to an element $\zeta^\infty \in L^2([0,1], X)$. Hence, with a slight abuse of notation, we conclude that

$$\boldsymbol{\nu}^n \rightharpoonup \boldsymbol{\nu}^\infty \quad \text{and} \quad \zeta^n \rightharpoonup \zeta^\infty \quad \text{as } n \to \infty.$$

The aim is now to prove existence of minimisers by showing that $(\boldsymbol{\nu}^\infty, \zeta^\infty)$ is a minimiser to $\mathcal{J}_{\gamma,\tau}(\,\cdot\,; g)\colon L^2([0,1], V \times X) \to \mathbb{R}$.

Before proceeding, we introduce some notation in order to simplify the expressions. Define

$$I_t^n := I_t^{\boldsymbol{\nu}^n, \zeta^n} \quad \text{and} \quad \varphi_{s,t}^n := \varphi_{s,t}^{\boldsymbol{\nu}^n} \quad \text{for } n \in \mathbb{N} \cup \{\infty\}. \tag{10}$$

Hence, assuming geometric group action (4) and using (2), we can write

$$\mathcal{J}_{\gamma,\tau}(\boldsymbol{\nu}^n, \zeta^n; g) = \frac{\gamma}{2}\|\boldsymbol{\nu}^n\|_2^2 + \frac{\tau}{2}\|\zeta^n\|_2^2 + \mathcal{L}\Big(\mathcal{A}\big(I_1^n \circ \varphi_{1,0}^n\big), g\Big)$$

for $n \in \mathbb{N} \cup \{\infty\}$. Assume next that the following holds:

$$I_1^n \circ \varphi_{1,0}^n \rightharpoonup I_1^\infty \circ \varphi_{1,0}^\infty \quad \text{as } n \to \infty. \tag{11}$$

The data discrepancy term $\mathcal{L}(\,\cdot\,, g)\colon Y \to \mathbb{R}$ is weakly lower semi continuous and the forward operator $\mathcal{A}\colon X \to Y$ is continuous, so $\mathcal{L}(\,\cdot\,, g) \circ \mathcal{A}$ is also weakly lower semi continuous and then (11) implies

$$\mathcal{L}\big(\mathcal{A}(I_1^\infty \circ \varphi_{1,0}^\infty), g\big) \le \liminf_{n\to\infty} \mathcal{L}(\mathcal{A}(I_1^n \circ \varphi_{1,0}^n), g). \tag{12}$$

Furthermore, from the weak convergences of $\boldsymbol{\nu}^n$ and ζ^n, we get

$$\frac{\gamma}{2}\|\boldsymbol{\nu}^\infty\|_2^2 + \frac{\tau}{2}\|\zeta^\infty\|_2^2 \le \liminf_{n\to\infty} \Big[\frac{\gamma}{2}\|\boldsymbol{\nu}^n\|_2^2 + \frac{\tau}{2}\|\zeta^n\|_2^2\Big]. \tag{13}$$

Hence, combining (12) and (13) we obtain

$$\mathcal{J}_{\gamma,\tau}(\boldsymbol{\nu}^\infty, \zeta^\infty; g) \le \lim_{n\to\infty} \mathcal{J}_{\gamma,\tau}(\boldsymbol{\nu}^n, \zeta^n; g).$$

Since $\{(\boldsymbol{\nu}^n, \zeta^n)\}_n \subset L^2([0,1], V \times X)$ is a minimising sequence, this yields

$$\mathcal{J}_{\gamma,\tau}(\boldsymbol{\nu}^\infty, \zeta^\infty; g) = \inf_{(\boldsymbol{\nu},\zeta) \in L^2([0,1], V\times X)} \mathcal{J}_{\gamma,\tau}(\boldsymbol{\nu}, \zeta; g),$$

which proves $(\boldsymbol{\nu}^\infty, \zeta^\infty) \in L^2([0,1], V \times X)$ is a minimiser to $\mathcal{J}_{\gamma,\tau}(\,\cdot\,; g)$.

Hence, to finalize the proof we need to show that (11) holds. We start by observing that the solution of (7) can be written as

$$I_t^n := I_0^n(x) + \int_0^t \zeta^n\big(s, \varphi_{0,s}^n(x)\big)\mathrm{d}s \quad \text{for } n \in \mathbb{N} \cup \{\infty\}, \tag{14}$$

and note that $(t,x) \mapsto I_t^n(x) \in C([0,1] \times \Omega, \mathbb{R})$. Next, we claim that

$$I_1^n \rightharpoonup I_1^\infty \quad \text{for some } I_1^\infty \in X,$$

which is equivalent to

$$\lim_{n\to\infty} \langle I_1^n - I_1^\infty, J\rangle = 0 \quad \text{for any } J \in L^2(\Omega, \mathbb{R}). \tag{15}$$

To prove (15), note first that since continuous functions are dense in L^2, it is enough to show (15) holds for $J \in C_0(\Omega, \mathbb{R})$. Next,

$$\begin{aligned}
\langle I_1^n - I_1^\infty, J\rangle &= \int_\Omega \int_0^t \Big(\zeta^n\big(s, \varphi_{0,s}^n(x)\big) - \zeta^\infty\big(s, \varphi_{0,s}^\infty(x)\big)\Big) J(x)\mathrm{d}s\mathrm{d}x && (16)\\
&= \int_\Omega \int_0^t \Big(\zeta^n\big(s, \varphi_{0,s}^n(x)\big) - \zeta^n\big(s, \varphi_{0,s}^\infty(x)\big)\Big) J(x)\mathrm{d}s\mathrm{d}x && (17)\\
&\quad + \int_\Omega \int_0^t \Big(\zeta^n\big(s, \varphi_{0,s}^n(x)\big) - \zeta^\infty\big(s, \varphi_{0,s}^\infty(x)\big)\Big) J(x)\mathrm{d}s\mathrm{d}x. && (18)
\end{aligned}$$

Let us now take a closer look at the term in (17):

$$\begin{aligned}
&\int_\Omega \int_0^t \Big(\zeta^n\big(s, \varphi_{0,s}^n(x)\big) - \zeta^n\big(s, \varphi_{0,s}^\infty(x)\big)\Big) J(x)\mathrm{d}s\mathrm{d}x\\
&\quad = \int_\Omega \int_0^t \zeta^n(s,x) J\big(\varphi_{0,s}^n(x)\big)\big|D\varphi_{0,s}^n(x)\big|\mathrm{d}s\mathrm{d}x\\
&\qquad\qquad - \int_\Omega \int_0^t \zeta^\infty(s,x) J\big(\varphi_{0,s}^\infty(x)\big)\big|D\varphi_{0,s}^\infty(x)\big|\mathrm{d}s\mathrm{d}x\\
&\quad = \int_\Omega \int_0^t \zeta^n(s,x)\Big(J\big(\varphi_{0,s}^n(x)\big)\big|D\varphi_{0,s}^n(x)\big| - J\big(\varphi_{0,s}^\infty(x)\big)\big|D\varphi_{0,s}^\infty(x)\big|\Big)\mathrm{d}s\mathrm{d}x\\
&\qquad - \int_\Omega \int_0^t \Big(\zeta^\infty(s,x) - \zeta^n(s,x)\Big) J\big(\varphi_{0,s}^\infty(x)\big)\big|D\varphi_{0,s}^\infty(x)\big|\mathrm{d}s\mathrm{d}x\\
&\qquad\qquad = \langle \zeta^n, J^n - J^\infty\rangle - \langle \zeta^\infty - \zeta^n, J^\infty\rangle
\end{aligned}$$

where $J^n \in L^2([0,1], X)$ is defined as

$$J^n(s,x) := J\big(\varphi_{s,0}^n(x)\big)\big|D\varphi_{s,0}^n(x)\big| \quad \text{for } n \in \mathbb{N} \cup \{\infty\}. \tag{19}$$

By proposition 3 we know that $\varphi_{s,0}^n \to \varphi_{s,0}^\infty$ and $D\varphi_{s,0}^n \to D\varphi_{s,0}^\infty$ uniformly on Ω. Since J is continuous on Ω, we conclude that $\|J^n - J^\infty\|_2 \to 0$. When combined with the boundedness of ζ^n, we get

$$\langle \zeta^n, J^n - J^\infty\rangle \le \|\zeta^n\|_2 \cdot \|J^n - J^\infty\|_2 \to 0.$$

Furthermore, since $\zeta^n \rightharpoonup \zeta^\infty$, we also get $\langle \zeta^\infty - \zeta^n, J^\infty \rangle \to 0$. Hence, we have shown that (17) tends to zero, i.e.,

$$\lim_{n\to\infty} \int_\Omega \int_0^t \Big(\zeta^n\big(s, \varphi^n_{0,s}(x)\big) - \zeta^n\big(s, \varphi^\infty_{0,s}(x)\big) \Big) J(x) \mathrm{d}s\mathrm{d}x = 0.$$

Finally, we consider the term in (18). Since $\zeta^n \rightharpoonup \zeta^\infty$, we immediately obtain

$$\int_\Omega \int_0^t \Big(\zeta^n\big(s, \varphi^\infty_{s}(x)\big) - \zeta^\infty\big(s, \varphi^\infty_{s}(x)\big) \Big) J(x) \mathrm{d}s\mathrm{d}x = \big\langle \zeta^n - \zeta^\infty, J^\infty \big\rangle \to 0.$$

To summarise, we have just proved that both terms (17) and (18) tend to 0 as $n \to \infty$, which implies that (15) holds, i.e., $I_1^n \rightharpoonup I_1^\infty$.

To prove (11), i.e., $I_1^n \circ \varphi^n_{1,0} \rightharpoonup I_1^\infty \circ \varphi^\infty_{1,0}$, we need to show that

$$\lim_{n\to\infty} \big\langle I_1^n \circ \varphi^n_{1,0} - I_1^\infty \circ \varphi^\infty_{1,0}, J \big\rangle = 0 \quad \text{for any } J \in L^2(\Omega, \mathbb{R}), \tag{20}$$

and as before, we may assume $J \in C_0(\Omega, \mathbb{R})$. Using (19) we can express the term in (20) whose limit we seek as

$$\begin{aligned} &\big| \langle I_1^n \circ \varphi^n_{1,0} - I_1^\infty \circ \varphi^\infty_{1,0}, J \rangle \big| \\ &\qquad \le \Big| \big\langle I_1^n, J^n(1, \,\cdot\,) - J^\infty(1, \,\cdot\,) \big\rangle \Big| + \Big| \big\langle I_1^n - I_1^\infty, J^\infty(1, \,\cdot\,) \big\rangle \Big| \\ &\qquad\qquad \le \|I_1^n\| \cdot \big\| J^n(1, \,\cdot\,) - J^\infty(1, \,\cdot\,) \big\| + \big| \langle I_1^n - I_1^\infty, J^\infty(1, \,\cdot\,) \rangle \big|. \end{aligned}$$

Since $\|I_1^n\|$ is bounded (because $\|\zeta^n\|$ is bounded) and since $I_1^n \rightharpoonup I_1^\infty$ (which we shoed before), all terms above tend to 0 as $n \to \infty$, i.e., (20) holds.

This concludes the proof of (11), which in turn implies the existence of a minimiser of $\mathcal{J}_{\gamma,\tau}(\,\cdot\,; g)$. □

Our next result shows stability in the sense that the solution to the indirect registration problem is (weakly) continuous w.r.t. variations in data.

Proposition 5 (Stability)**.** *Let $\{g_k\}_k \subset Y$ and assume this sequence converges (in norm) to some $g \in Y$. Next, for each $\gamma, \tau > 0$ and each k, define $(\boldsymbol{\nu}^k, \zeta^k) \in L^2\left([0,1], V \times X\right)$ as*

$$(\boldsymbol{\nu}^k, \zeta^k) = \operatorname*{arg\,min}_{(\boldsymbol{\nu}, \zeta)} \mathcal{J}_{\gamma,\tau}(\boldsymbol{\nu}, \zeta; g_k).$$

Then there exists a sub sequence of $(\boldsymbol{\nu}^k, \zeta^k)$ that converges weakly to a minimiser of $\mathcal{J}_{\gamma,\tau}(\,\cdot\,; g)$ in (8).

Proof. $\mathcal{J}_{\gamma,\tau}(\,\cdot\,; g_k)$ has a minimiser $(\boldsymbol{\nu}^k, \zeta^k) \in L^2\left([0,1], V \times X\right)$ for any $g_k \in Y$ (proposition 4). The idea is first to show that the sequences $(\boldsymbol{\nu}^k)_k$ and $(\zeta^k)_k$ are bounded. Next, we show that there exists a weakly converging

subsequence of $(\boldsymbol{\nu}^k, \zeta^k)$ that converges to a minimiser $(\boldsymbol{\nu}, \zeta)$ of $\mathcal{J}_{\gamma,\tau}(\,\cdot\,; g)$, which also exists due to proposition 4.

Since $(\boldsymbol{\nu}^k, \zeta^k)$ minimises $\mathcal{J}_{\gamma,\tau}(\,\cdot\,; g_k)$, we have by (8) that

$$\|\boldsymbol{\nu}^k\|_2^2 \leq \frac{2}{\gamma}\,\mathcal{J}_{\gamma,\tau}(\,\cdot\,; g_k)(\boldsymbol{\nu}^k, \zeta^k) \leq \frac{2}{\gamma}\,\mathcal{J}_{\gamma,\tau}(\,\cdot\,; g_k)(\mathbf{0}, 0) \quad \text{for each } k. \tag{21}$$

Observe now that if $\boldsymbol{\nu} = \mathbf{0}$ and $\zeta = 0$, then $\varphi_{0,1}^{\boldsymbol{\nu}} = \mathrm{Id}$ by (1) and $I_1^{\boldsymbol{\nu},\zeta} = I_0$ by (7), so in particular

$$\mathcal{W}\big(\varphi_{0,1}^{\boldsymbol{\nu}}, I_1^{\boldsymbol{\nu},\zeta}\big)\big) = I_0 \quad \text{whenever } \boldsymbol{\nu} = \mathbf{0} \text{ and } \zeta = 0.$$

Hence, $\mathcal{J}_{\gamma,\tau}(\,\cdot\,; g_k)(\mathbf{0}, 0) = \mathcal{L}\big(\mathcal{A}(I_0), g_k\big)$ and, in addition, $\|\boldsymbol{\nu}\|_2 = 0$ and $\|\zeta\|_2 = 0$, so (21) becomes

$$\|\boldsymbol{\nu}^k\|_2^2 \leq \frac{2}{\gamma}\,\mathcal{L}\big(\mathcal{A}(I_0), g_k\big) \to \mathcal{L}(\mathcal{A}(I_0), g) \quad \text{as } k \to \infty. \tag{22}$$

In conclusion, the sequence $(\boldsymbol{\nu}^k)_k \subset L^2\left([0,1], V\right)$ is bounded. In a similar way, we can show that $(\zeta^k)_k \subset L^2\left([0,1], X\right)$ is bounded.

The boundedness of both sequences implies that there are sub sequences to these that converge weakly to some elements $\boldsymbol{\nu}^\infty \in L^2\left([0,1], V\right)$ and $\zeta^\infty \in L^2\left([0,1], X\right)$, respectively. Thus, to complete the proof, we need to show that $(\boldsymbol{\nu}^\infty, \zeta^\infty) \in L^2\left([0,1], V \times X\right)$ minimises $\mathcal{J}_{\gamma,\tau}(\,\cdot\,; g)$, i.e., that

$$\mathcal{J}_{\gamma,\tau}(\boldsymbol{\nu}^\infty, \zeta^\infty; g) \leq \mathcal{J}_{\gamma,\tau}(\boldsymbol{\nu}, \zeta; g) \quad \text{holds for any } (\boldsymbol{\nu}, \zeta) \in L^2\left([0,1], V \times X\right).$$

From the weak convergences, we obtain

$$\begin{aligned}\frac{\gamma}{2}\|\boldsymbol{\nu}^\infty\|_2^2 + \frac{\tau}{2}\|\zeta^\infty\|_2^2 &\leq \frac{\gamma}{2}\liminf_k \|\boldsymbol{\nu}^k\|_2^2 + \frac{\tau}{2}\liminf_k \|\zeta^k\|_2^2 \\ &\leq \frac{1}{2}\liminf_k \Big[\gamma\|\boldsymbol{\nu}^k\|_2^2 + \tau\|\zeta^k\|_2^2\Big]. \end{aligned} \tag{23}$$

The weak convergence also implies (see proof of proposition 4) that

$$\mathcal{W}\big(\varphi_{0,1}^k, I_1^\infty\big) \rightharpoonup \mathcal{W}\big(\varphi_{0,1}^\infty, I_1^\infty\big) \quad \text{in } X.$$

In the above, we have used the notational convention introduced in (10). By the lower semi-continuity of $\mathcal{L}$, we get

$$\mathcal{L}\Big(\mathcal{A}\big(\mathcal{W}(\varphi_{0,1}^\infty, I_1^\infty)\big), g\Big) \leq \liminf_k \mathcal{L}\Big(\mathcal{A}\big(\mathcal{W}(\varphi_{0,1}^k, I_1^k)\big), g_k\Big). \tag{24}$$

Hence,

$$\begin{aligned}\mathcal{J}_{\gamma,\tau}(\boldsymbol{\nu}^\infty, \zeta^\infty; g) &= \frac{\gamma}{2}\|\boldsymbol{\nu}^\infty\|_2^2 + \frac{\tau}{2}\|\zeta^\infty\|_2^2 + \mathcal{L}\Big(\mathcal{A}\big(\mathcal{W}(\varphi_{0,1}^\infty, I_1^\infty)\big), g\Big). \\ &\leq \frac{1}{2}\liminf_k \Big[\gamma\|\boldsymbol{\nu}^k\|_2^2 + \tau\|\zeta^k\|_2^2\Big] + \liminf_k \mathcal{L}\Big(\mathcal{A}\big(\mathcal{W}(\varphi_{0,1}^k, I_1^k)\big), g_k\Big) \\ &\leq \liminf_k \mathcal{J}_{\gamma,\tau}(\boldsymbol{\nu}^k, \zeta^k; g_k). \end{aligned} \tag{25}$$

Next, since $(\boldsymbol{\nu}^k, \zeta^k) \in L^2([0,1], V \times X)$ minimises $\mathcal{J}_{\gamma,\tau}(\,\cdot\,; g_k)$, we get

$$\mathcal{J}_{\gamma,\tau}(\boldsymbol{\nu}^\infty, \zeta^\infty; g) \leq \liminf_k \mathcal{J}_{\gamma,\tau}(\boldsymbol{\nu}, \zeta; g_k) \text{ for any } (\boldsymbol{\nu}, \zeta) \in L^2([0,1], V \times X).$$

Furthermore, $\mathcal{J}_{\gamma,\tau}(\boldsymbol{\nu}, \zeta; g_k) \to \mathcal{J}_{\gamma,\tau}(\boldsymbol{\nu}, \zeta; g)$, so

$$\mathcal{J}_{\gamma,\tau}(\boldsymbol{\nu}^\infty, \zeta^\infty; g) \leq \mathcal{J}_{\gamma,\tau}(\boldsymbol{\nu}, \zeta; g) \quad \text{for all } (\boldsymbol{\nu}, \zeta) \in L^2([0,1], V \times X).$$

In particular, we have shown that $(\boldsymbol{\nu}^\infty, \zeta^\infty)$ minimises $\mathcal{J}_{\gamma,\tau}(\,\cdot\,; g)$. □

Our final results concerns convergence, which investigates the behaviour of the solution as data error tends to zero and regularisation parameters are adapted accordingly through a parameter choice rule against the data error.

Proposition 6 (Convergence)**.** *Let $g \in Y$ and assume*

$$\mathcal{A}\big(\mathcal{W}(\varphi_{0,1}^{\boldsymbol{\nu}}, I_1^{\boldsymbol{\nu},\zeta})\big) = g \quad \textit{for some } (\boldsymbol{\nu}, \zeta) \in L^2([0,1], V \times X).$$

Next, for parameter choice rules $\delta \mapsto \gamma(\delta)$ and $\delta \mapsto \tau(\delta)$ with $\delta > 0$, define

$$(\boldsymbol{\nu}_\delta, \zeta_\delta) \in \operatorname*{arg\,min}_{(\boldsymbol{\nu},\zeta)} \mathcal{J}_{\gamma(\delta),\tau(\delta)}(\boldsymbol{\nu}, \zeta; g + e_\delta)$$

where $e_\delta \in Y$ (data error) has magnitude $\|e_\delta\| \leq \delta$. Finally, assume that $\delta \mapsto \gamma(\delta)/\tau(\delta)$ and $\delta \mapsto \tau(\delta)/\gamma(\delta)$ are bounded, and

$$\lim_{\delta\to 0} \gamma(\delta) = \lim_{\delta\to 0} \tau(\delta) = \lim_{\delta\to 0} \frac{\delta^2}{\gamma(\delta)} = \lim_{\delta\to 0} \frac{\delta^2}{\tau(\delta)} = 0.$$

Then, for any sequence $\delta_k \to 0$ there exists a sub-sequence $\delta_{k'}$ such that $(\boldsymbol{\nu}_{\delta_{k'}}, \zeta_{\delta_{k'}})$ converges weakly to a $(\boldsymbol{\nu}^*, \zeta^*)$ satisfying $\mathcal{A}\big(\mathcal{W}(\varphi_{0,1}^{\boldsymbol{\nu}^*}, I_1^{\boldsymbol{\nu}^*,\zeta^*})\big) = g$.

Proof. Let (δ_k) be a sequence converging to 0 and, for each k, let us denote

$$g_k := g + e_{\delta_k}, \quad \boldsymbol{\nu}^k := \boldsymbol{\nu}_{\delta_k}, \quad \text{and} \quad \zeta^k := \zeta_{\delta_k}.$$

Similarly to previous proofs, we will show that the sequences $(\boldsymbol{\nu}^k)$ and (ζ^k) are bounded, and then that the weakly converging subsequence that can be extracted from $(\boldsymbol{\nu}^k, \zeta^k)$ converges to a suitable solution.

Define $\gamma_k := \gamma(\delta_k)$ and $\tau_k := \gamma(\delta_k)$. Then, for each k we have

$$\begin{aligned}\|\boldsymbol{\nu}^k\|_2^2 &\leq \frac{1}{\gamma_k}\,\mathcal{J}_{\gamma_k,\tau_k,g_k}(\boldsymbol{\nu}^k, \zeta^k) \leq \frac{1}{\gamma_k}\,\mathcal{J}_{\gamma_k,\tau_k,g_k}(\widehat{\boldsymbol{\nu}}, \hat{\zeta}) \\ &= \frac{1}{\gamma_k}\Big(\gamma_k\|\widehat{\boldsymbol{\nu}}\|_2^2 + \tau_k\|\hat{\zeta}\|_2^2 + \mathcal{L}(g, g_k)\Big) \leq \|\widehat{\boldsymbol{\nu}}\|_2^2 + \frac{\tau_k}{\gamma_k}\|\hat{\zeta}\|_2^2 + \frac{\delta_k}{\gamma_k}.\end{aligned}$$

From the assumptions on the parameter choice rules, we conclude that $(\boldsymbol{\nu}^k) \subset L^2([0,1], V)$ is bounded. Similarly, one can show that $(\zeta^k) \subset L^2([0,1], X)$ is bounded.

From the above, we conclude that there is a subsequence of $(\boldsymbol{\nu}^k, \zeta^k)$ that converges weakly to $(\widetilde{\boldsymbol{\nu}}, \widetilde{\zeta})$ in $L^2([0,1], V) \times L^2([0,1], V)$. Then (see proof of proposition 4)

$$\mathcal{L}\Big(\mathcal{A}\big(\mathcal{W}(\varphi_{0,1}^{\widetilde{\boldsymbol{\nu}}}, I_1^{\widetilde{\boldsymbol{\nu}},\widetilde{\zeta}})\big), g\Big) \leq \liminf_k \mathcal{L}\Big(\mathcal{A}\big(\mathcal{W}\big(\varphi_{0,1}^{\boldsymbol{\nu}_k}, I_1^{\widetilde{\boldsymbol{\nu}},\widetilde{\zeta}}\big)\big), g_k\Big).$$

Furthermore, the above quantity converges to 0 since

$$\begin{aligned}\mathcal{L}\Big(\mathcal{A}\big(\mathcal{W}(\varphi_{0,1}^{\boldsymbol{\nu}^k}, I_1^{\boldsymbol{\nu}^k,\zeta^k})\big), g_k\Big) &\leq \mathcal{J}_{\gamma_k,\tau_k,g_k}(\boldsymbol{\nu}^k, \zeta^k) \leq \mathcal{J}_{\gamma_k,\tau_k,g_k}(\widehat{\boldsymbol{\nu}}, \hat{\zeta}) \\ &= \gamma_k \|\widehat{\boldsymbol{\nu}}\|_2^2 + \tau_k \|\hat{\zeta}\|_2^2 + \mathcal{L}(g, g_k) \to 0 \quad \text{and } k \to \infty.\end{aligned}$$

Hence, $\mathcal{A}\big(\mathcal{W}(\varphi_{0,1}^{\widetilde{\boldsymbol{\nu}}}, I_1^{\widetilde{\boldsymbol{\nu}},\widetilde{\zeta}})\big) = g$. □

4.4 Numerical implementation

In order to solve (9), we use a gradient descent scheme on the control variable $(\boldsymbol{\nu}, \zeta) \in L^2([0,1], V \times X)$ with a uniform discretisation of the interval $[0,1]$ into N parts, i.e., $t_i = 1/N$ for $i = 0, \ldots, N$ and the gradient descent is performed on $\big(\boldsymbol{\nu}(t_i, \cdot), \zeta(t_i, \cdot)\big)$, for $i = 0, 1, \ldots, N$.

we use a Euler scheme on this discretisation for computing the numerical integrations. The flow equation (1) is computed using the following approximation with small deformations:

$$\varphi_{t_i,0}^{\boldsymbol{\nu}} \approx \varphi_{t_{i-1},0}^{\boldsymbol{\nu}} \circ \Big(\mathrm{Id} - \frac{1}{N}\boldsymbol{\nu}(t_{i-1}, \cdot)\Big).$$

Algorithm 1 presents the implementation[2] for computing the gradient of $\mathcal{J}$ based on expressions from appendix A. Note that the number 'N' is not a fixed value, which is just a value for numerical discretisation. As long as such value is sufficiently large, we can obtain a small linearised diffeomorphic deformation. Then the large diffeomorphic deformation can be obtained by compositions of these small linearised deformations [40]. The computation of the Jacobian determinant $\big|\mathrm{D}\varphi_{t_i,1}^{\boldsymbol{\nu}}(x)\big|$ at each time point is based on the following approximation similar to the one used in [11]:

$$\big|\mathrm{D}\varphi_{t_i,1}^{\boldsymbol{\nu}}(\cdot)\big| \approx \Big(1 + \frac{1}{N}\operatorname{div}\boldsymbol{\nu}(t_i, \cdot)\Big)\big|\mathrm{D}\varphi_{t_{i+1},1}^{\boldsymbol{\nu}}\big| \circ \Big(\mathrm{Id} + \frac{1}{N}\boldsymbol{\nu}(t_i, \cdot)\Big).$$

By simple derivations for the 2D case, we have

$$\begin{aligned}\Big|\mathrm{D}\varphi_{t_i,1}^{\boldsymbol{\nu}}(\cdot)\Big| = \Big(1 + \frac{1}{N}\operatorname{div}\boldsymbol{\nu}(t_i, \cdot) + \frac{1}{N^2}|\mathrm{D}\boldsymbol{\nu}(t_i, \cdot)|\Big)\big|\mathrm{D}\varphi_{t_{i+1},1}^{\boldsymbol{\nu}}\big| \circ \\ \Big(\mathrm{Id} + \frac{1}{N}\boldsymbol{\nu}(t_i, \cdot)\Big).\end{aligned}$$

[2] https://github.com/bgris/IndirectMatchingMetamorphosis

It is easy to see that the error is about $O(N^{-2})$ for the above approximation.

Since all of the numerical implementations are based on the discretisations in temporal and spatial domains, the exact computation to the Jacobian determinant is hardly required. Even if we use the exact one, it might not increase the overall precision of the algorithm. Moreover, if the N is large enough, this error can be neglected.

5 Application to 2D tomography

5.1 The setting

Let $X = L^2(\Omega, \mathbb{R})$ and its elements represent 2D images on a fixed bounded domain $\Omega \subset \mathbb{R}^2$. In the application shown here, diffeomorphisms act on X through the geometric group action in (4). The goal is to register a given differentiable template image $I_0 \in X$ against a target that observed indirectly as in (5).

The forward operator The forward operator $\mathcal{A}\colon X \to Y$ in 2D tomographic imaging is the 2D ray/Radon transform, i.e.,

$$\mathcal{A}(f)(\omega, x) = \int_{\mathbb{R}} f(x + s\omega)\mathrm{d}s \quad \text{for } \omega \in S^1 \text{ and } x \in \omega^\perp.$$

Here, S^1 is the unit circle, so (ω, x) encodes the line $s \mapsto x + s\omega$ in $\mathbb{R}^2$ with direction ω through x. The data manifold M is the set of such lines that are included in the measurements, i.e., M is given by the experimental set-up, so $Y = L^2(M, \mathbb{R})$. We will consider parallel lines in $\mathbb{R}^2$ (parallel beam data), i.e., tomographic data $g \in Y$ are noisy digitised values of an L^2-function on this manifold. The forward operator is linear, so it is Gateaux differentiable and the adjoint of its derivative is given by the backprojection [27, 24].

The squared 2-norm corresponds to the data likelihood when data is corrupted by additive Gaussian noise:

$$\mathcal{L}\colon Y \times Y \to \mathbb{R} \quad \text{with} \quad \mathcal{L}(g, h) = \|g - h\|_2^2.$$

The noise level in data is specified by the peak signal-to-noise ratio (PSNR), which is defined as

$$\mathrm{PSNR}(g) = 10 \log_{10}\left(\frac{\|g_0 - \overline{g_0}\|^2}{\|e - \overline{e}\|^2}\right) \quad \text{for } g = g_0 + e.$$

In the above, g_0 is the noise-free part and e is the noise component of data with $\overline{g_0}$ and $\overline{e}$ denoting the mean of g_0 and e, respectively. The PSNR is expressed in terms of dB.

Algorithm 1 Computation of $\nabla\,\mathcal{J}(\boldsymbol{\nu},\zeta)$.

Require: $\boldsymbol{\nu}(t_i,\,\cdot\,)$ and $\zeta(t_i,\,\cdot\,)$ with $t_i \leftarrow i/N$ for $i = 0, 1, \dots, N$.

for $i = 1, \dots, N$ **do** ▷ Compute $\zeta(t_i,\,\cdot\,)\circ\varphi^{\boldsymbol{\nu}}_{0,t_i}$
  $temp \leftarrow \zeta(t_i,\,\cdot\,)$
  for $j = i-1, \dots, 0$ **do**
    $temp \leftarrow temp \circ \Big(\mathrm{Id} + \frac{1}{N}\boldsymbol{\nu}(t_j,\,\cdot\,)\Big)$
  end for
  $\zeta(t_i,\,\cdot\,)\circ\varphi^{\boldsymbol{\nu}}_{0,t_i} \leftarrow temp$
end for
for $i = 1, \dots, N$ **do** ▷ Compute $f^{\boldsymbol{\nu},\zeta}(t_i,\,\cdot\,) := I^{\boldsymbol{\nu},\zeta}(t_i,\,\cdot\,)\circ\varphi^{\boldsymbol{\nu}}_{t_i,0}$
  $I^{\boldsymbol{\nu},\zeta}(t_i,\,\cdot\,) \leftarrow I_0 + \sum_{j=0}^{i-1} I^{\boldsymbol{\nu},\zeta}(t_j,\,\cdot\,) + \frac{1}{N}\zeta(t_j,\,\cdot\,)\circ\varphi^{\boldsymbol{\nu}}_{0,t_j}$
  $I^{\boldsymbol{\nu},\zeta}(t_i,\,\cdot\,)\circ\varphi^{\boldsymbol{\nu}}_{0,0} \leftarrow I^{\boldsymbol{\nu},\zeta}(t_i,\,\cdot\,)$
  for $j = 1, \dots, i$ **do**
    $I^{\boldsymbol{\nu},\zeta}(t_i,\,\cdot\,)\circ\varphi^{\boldsymbol{\nu}}_{t_j,0} \leftarrow \big(I^{\boldsymbol{\nu},\zeta}(t_i,\,\cdot\,)\circ\varphi^{\boldsymbol{\nu}}_{0,t_{j-1}}\big)\circ\Big(\mathrm{Id} - \frac{1}{N}\boldsymbol{\nu}(t_{j-1},\,\cdot\,)\Big)$
  end for
end for
for $i = 1, \dots, N$ **do** ▷ Compute $I_0\circ\varphi^{\boldsymbol{\nu}}_{t_i,0}$
  $I_0\circ\varphi^{\boldsymbol{\nu}}_{0,0} \leftarrow I_0\circ\varphi^{\boldsymbol{\nu}}_{0,0} = I_0$
  $I_0\circ\varphi^{\boldsymbol{\nu}}_{t_i,0} \leftarrow \big(I_0\circ\varphi^{\boldsymbol{\nu}}_{t_{i-1},0}\big)\circ\Big(\mathrm{Id} - \frac{1}{N}\boldsymbol{\nu}(t_{i-1},\,\cdot\,)\Big)$
end for
for $i = 1, \dots, N$ **do**
  $G(t_i,\,\cdot\,) \leftarrow \nabla(I_0\circ\varphi^{\boldsymbol{\nu}}_{t_i,0}) + \sum_{j=0}^{t_{i-1}} \frac{1}{N}\nabla(\zeta(t_j,\cdot)\circ\varphi^{\boldsymbol{\nu}}_{t_i,t_j})$
end for
$\big|\,\mathrm{D}\varphi^{\boldsymbol{\nu}}_{t_N,1}\big| = \big|\,\mathrm{D}\varphi^{\boldsymbol{\nu}}_{1,1}\big| = 1$ ▷ Compute $\big|\,\mathrm{D}\varphi^{\boldsymbol{\nu}}_{t_i,1}\big|$
for $i = N-1, \dots, 0$ **do**
  $\big|\,\mathrm{D}\varphi^{\boldsymbol{\nu}}_{t_i,1}\big| \leftarrow \Big(1 + \frac{1}{N}\operatorname{div}\boldsymbol{\nu}(t_i,\,\cdot\,)\Big)\big|\,\mathrm{D}\varphi^{\boldsymbol{\nu}}_{t_{i+1},1}\big|\circ\Big(\mathrm{Id} + \frac{1}{N}\boldsymbol{\nu}(t_i,\,\cdot\,)\Big)$
end for
$\nabla\,\mathcal{L}\big(f^{\boldsymbol{\nu},\zeta}(1,\,\cdot\,),g\big)\big(\varphi^{\boldsymbol{\nu}}_{t_N,1}\big) \leftarrow \nabla\,\mathcal{L}\big(f^{\boldsymbol{\nu},\zeta}(1,\,\cdot\,),g\big)$
for $i = N-1, \dots, 0$ **do** ▷ Compute $\nabla\,\mathcal{L}\big(f^{\boldsymbol{\nu},\zeta}(1,\,\cdot\,),g\big)\big(\varphi^{\boldsymbol{\nu}}_{t_i,1}\big)$
  $\nabla\,\mathcal{L}\big(f^{\boldsymbol{\nu},\zeta}(1,\,\cdot\,),g\big)\big(\varphi^{\boldsymbol{\nu}}_{t_i,1}\big) \leftarrow \nabla\,\mathcal{L}\big(f^{\boldsymbol{\nu},\zeta}(1,\,\cdot\,),g\big)\big(\varphi^{\boldsymbol{\nu}}_{t_{i+1},1}\big)\circ\Big(\mathrm{Id} + \frac{1}{N}\boldsymbol{\nu}(t_i,\,\cdot\,)\Big)$
end for
for $i = 1, \dots, N$ **do** ▷ Compute $\nabla\,\mathcal{J}(\boldsymbol{\nu},\zeta)$

$$\nabla_{\boldsymbol{\nu}}\,\mathcal{J}_{\gamma,\tau}(\boldsymbol{\nu},\zeta,g)(t_i,,\,\cdot\,) \leftarrow 2\gamma\boldsymbol{\nu}(t_i,,\,\cdot\,) - \int_\Omega K(x,\,\cdot\,)\Big|\mathrm{Det}(\mathrm{d}\varphi^{\boldsymbol{\nu}}_{t_i,1}(x))\Big|\nabla\,\mathcal{L}\big(f^{\boldsymbol{\nu},\zeta}(1,\,\cdot\,),g\big)\big(\varphi^{\boldsymbol{\nu}}_{t_i,1}(x)\big)G(t_i,x)\mathrm{d}x$$

$$\nabla_{\zeta}\,\mathcal{J}_{\gamma,\tau}(\boldsymbol{\nu},\zeta)(t_i,,\,\cdot\,) \leftarrow 2\tau\zeta(t_i,,\,\cdot\,) + |\,\mathrm{Det}(\mathrm{d}\varphi^{\boldsymbol{\nu}}_{t_i,1})\Big|\nabla\,\mathcal{L}\big(f^{\boldsymbol{\nu},\zeta}(1,\,\cdot\,),g\big)\big(\varphi^{\boldsymbol{\nu}}_{t_i,1}(x)\big)G(t_i,\,\cdot\,)$$

end for
return $\nabla\,\mathcal{J}(\boldsymbol{\nu})(t_i,\,\cdot\,)$, $\nabla\,\mathcal{J}(\zeta)(t_i,\,\cdot\,)$ for $i = 1, \dots, N$.

Joint tomographic reconstruction and registration Under the geometric group action (4), metamorphosis based-indirect registration reads as

$$f_1^{\widehat{\boldsymbol{\nu}},\widehat{\zeta}} = \mathcal{W}\big(\varphi_{0,1}^{\widehat{\boldsymbol{\nu}}}, I_1^{\widehat{\boldsymbol{\nu}},\widehat{\zeta}}\big) = I_1^{\widehat{\boldsymbol{\nu}},\widehat{\zeta}} \circ \varphi_{1,0}^{\widehat{\boldsymbol{\nu}}}$$

where $(\widehat{\boldsymbol{\nu}}, \widehat{\zeta}) \in L^2\left([0,1], V \times X\right)$ minimises (8), i.e., given regularisation parameters $\gamma, \tau \geq 0$ and initial template $I_0 \in X$ we solve

$$\min_{(\boldsymbol{\nu},\zeta)} \left[\frac{\gamma}{2}\|\boldsymbol{\nu}\|_2^2 + \frac{\tau}{2}\|\zeta\|_2^2 + \left\| \mathcal{A}\Big(f\big(1, \phi(1, \,\cdot\,)^{-1}\big)\Big) - g \right\|_2^2 \right]$$

$$\begin{cases} \dfrac{\mathrm{d}}{\mathrm{d}t} f(t,x) = \zeta\big(t, \phi(t,x)\big) \\ f(0,x) = I_0(x) \\ \dfrac{d}{dt}\phi(t,x) = \boldsymbol{\nu}\big(t, \phi(t,x)\big) \\ \phi(0,x) = x. \end{cases} \tag{26}$$

We will consider a set V of vector fields that is an RKHS with a reproducing kernel represented by symmetric and positive definite Gaussian. Then V is admissible and is continuously embedded in $L^2(\Omega, \mathbb{R}^2)$. The kernel we pick is $K_\sigma \colon \Omega \times \Omega \to \mathbb{R}_+^{2\times 2}$

$$K_\sigma(x,y) := \exp\Big(-\frac{1}{2\sigma^2}\|x-y\|_2\Big) \begin{pmatrix} 1 & 0 \\ 0 & 1 \end{pmatrix} \quad \text{for } x, y \in \mathbb{R}^2 \text{ and } \sigma > 0. \tag{27}$$

The kernel-size σ also acts as a regularisation parameter.

5.2 Overview of experiments

In the following we test various aspects of using metamorphoses based indirect registration for joint tomographic reconstruction and registration. The tomographic inverse problem along with characteristics of the data are outlined in section 5.1. The results are obtained by solving (26) via a gradient descent, see appendix A for the computation of the gradient of the objective. For each reconstruction, we list the number of angles of the parallel beam ray transform, the kernel-size σ in (27), and the two regularisation parameters $\gamma, \tau > 0$ appearing in the objective functional in (26).

The first test (section 5.3) aims to show how metamorphoses based indirect registration handles a template with intensities that differ from those of the target. Section 5.4 considers the ability to handle an initial template with a topology that does not match the target. This is essential when one has simultaneous geometric and topological changes. As an example, in spatiotemporal imaging it may very well be the case that geometric deformation

takes place simultaneously as new masses appear or disappear. Next, section 5.5 studies the robustness of the solutions with respect to variations in the regularisation parameters. Finally, section 5.6 shows how indirect registration through metamorphoses can be used to recover a temporal evolution of a given template registered against time series of data. This is an essential part of spatio-temporal tomographic reconstruction.

Sections 5.3 to 5.5 have a common setting in that grey scale images in the reconstruction space are discretised using 256×256 pixels supported in a rectangular region Ω. The tomographic data is noisy samples of the 2D parallel beam ray transform of the target sampled at 100 angles uniformly distributed angles in $[0, \pi]$ with 362 lines/angle. Data is corrupted with additive Gaussian noise with differing noise levels. In the last section 5.6 we add a Poisson noise to the data in order to avoid inverse crime [39] and also test robustness against misspecification of the noise model.

5.3 Consistent topology and inconsistent intensities

Here, topology of the template is consistent with that of the target, but intensities differ. The template, which is shown in fig. 2(a), is registered against tomographic data shown in fig. 2(c). The (unknown) target used to generate data is shown in fig. 2(b). Also, data has a noise level corresponding to a PSNR of 15.6 dB and the kernel size σ is set to 1/16:th of the side length of the image domain Ω. The final reconstruction is shown in fig. 2(h), which is to be compared against the target in fig. 2(b). Figure 2 also shows image, deformation and template trajectories.

We clearly see that metamorphosis based indirect registration can handle a template with wrong intensities. As a comparison, see fig. 1(c) for the corresponding LDDMM based indirect registration using the same template and data. Furthermore, the different trajectories also provides easy visual interpretation of the influence of geometric and intensity deformations.

5.4 Inconsistent topology and intensities

Here, both topology and intensities of the template differ from those in the target. The template, which is shown in fig. 3(a), is registered against tomographic data shown in fig. 3(c). The (unknown) target used for generating the data is shown in fig. 3(b). Also, data has a noise level corresponding to a PSNR of 10.6 dB and the kernel size σ is set to 1/16:th of the side length of the rectangular image domain Ω. The final reconstruction is shown in fig. 3(h), which is to be compared against the target in fig. 3(b). Figure 3 also shows image, deformation and template trajectories.

We clearly see that metamorphosis based indirect registration can handle a template where both intensities and the topology are wrong. In particular, we can see follow both the deformation of the template and the appearance

of the white disc.

5.5 Robustness

Metamorphosis based indirect registration, which amounts to solving (26), requires selecting three parameters: the kernel-size σ and the two regularisation parameters γ and τ. Here we study the influence of these parameters on the final registered image (reconstruction). We conclude that the reconstruction is *very robust* with respect to the choice of these three parameters. This is illustrated in figs. 4 and 5 where the reconstructed image is in the left-most column. The metamorphosis framework provides, in addition to this reconstruction, a decomposition into a template part and a deformation part. However, unlike reconstruction, the task of decomposition is sensitive to the choice of these parameters.

We first study the influence of the choice of the two regularisation parameters γ and τ by considering the setup in section 5.3 for varying choices of these parameters. Two *extremal* solutions are valid for the change of the shape of the triangles: it can be generated by a change in the intensity value, or by a geometric change. The first solutions is the optimal solution for $\gamma = 10^{-1}$ and $\tau = 10^{-5}$ (i.e., when the deformation part is more penalised than the change in the intensity value) and the second one for $\lambda = 10^{-5}$ and $\tau = 10^{-1}$. For intermediate choices of parameters, like $\gamma = 10^{-3}$ and $\tau = 10^{-3}$, the optimal solution is an intermediate one when these two effects combine. We present these results in fig. 4. We emphasis again that for all choices of parameters the reconstructed images are of good quality, only its decomposition into deformation and template parts varies.

Let us next study the influence of the choice of the kernel size σ. This parameter defines the characteristic scale for the allowed deformations: if σ is small, deformations of small areas of the template are favored, while if σ is large, bigger areas will be easily displaced. Apart from the visual perception, the reconstruction is quantitatively compared using structural similarity (SSIM) [38] and PSNR. Table 1 lists SSIM and PSNR values for reconstructions obtained using different choices of kernel size. We see that the *reconstruction is of good quality for all choices of kernel size* σ.

Interestingly, even if the reconstruction looks good, its decomposition into template and deformation is really different so the template and deformation parts seem to balance out each other in an non-intuitive way when they are combined to form the reconstruction. As an example, for extremal choices of the kernel size (like $\sigma \approx 1/3$ of the domain size), false structures appear in the template part of the decomposition. This is clearly an issue if the decomposition is used for interpretation. However these artefacts appear only for extremal choices of kernel size σ, it does not appear for values of the kernel size that lie between 1/32:nd and 1/6:th of the image size. We currently lack an understanding of this phenomenon.

σ	0.3	0.6	1	2	3	5	10
SSIM	0.660	0.703	0.737	0.769	0.766	0.764	0.682
PSNR	-7.75	-7.03	-6.57	-6.36	-6.49	-6.66	-8.98

Table 1: SSIM and PSNR values for metamorphosis based indirect registration with varying kernel size σ and fixed regularisation parameters $\gamma = \tau = 10^{-5}$.

5.6 Spatio-temporal reconstruction

The goal here is to recover the unknown temporal evolution of a template matched against (gated) parallel beam 2D ray transform data acquired at 10 different time points (from $t = 0.1$ to $t = 1$), so the target undergoes a temporal evolution. At each of the 10 time points, we only have limited tomographic data in the sense that i:th acquisition corresponds to sampling the parallel beam ray transform of the target at time t_i using 10 angles randomly distributed in $[(i-1)\pi/10, i\pi/10]$ using 362 lines/angles. We added a Poisson noise to these data. Similarly to previous experiments, the reconstruction space discretised as 256×256 pixel grey scale images supported in Ω.

The registration of the template I_0 against the temporal series of data g_i, $1 \leq i \leq 10$ at the 10 time points t_i is performed by minimising the following functional with respect to *one* trajectory $(\boldsymbol{\nu}, \zeta) \in L^2([0,1], V \times X)$:

$$\mathcal{J}_{\gamma,\tau}(\boldsymbol{\nu}, \zeta; g_1, \dots, g_{10}) := \frac{\gamma}{2}\|\boldsymbol{\nu}\|_2^2 + \frac{\tau}{2}\|\zeta\|_2^2 + \sum_{i=1}^{10} \mathcal{L}\Big(\mathcal{A}\big(\mathcal{W}(\varphi^{\boldsymbol{\nu}}_{0,t_i}, I^{\boldsymbol{\nu},\zeta}_{t_i})\big), g_i\Big)$$

where $t \mapsto I^{\boldsymbol{\nu},\zeta}_t$, is the absolutely continuous solution to

$$\begin{cases} \dfrac{\mathrm{d}}{\mathrm{d}t} I^{\boldsymbol{\nu},\zeta}_t(x) = \zeta\big(t, \varphi^{\boldsymbol{\nu}}_{0,t}(x)\big) \\ I^{\boldsymbol{\nu},\zeta}_0(x) = I_0(x) \end{cases} \qquad \text{with } \varphi^{\boldsymbol{\nu}}_{0,t} \in G_V \text{ as in (2).}$$

The target, the gated tomographic data, and the three trajectories (image, deformation and template) resulting from the metamorphosis based indirect registration are shown in fig. 6. We see that metamorphosis based indirect registration can be used for spatio-temporal reconstruction even when (gated) data is highly under sampled. In particular, we can recover the evolution (both the geometric deformation and the appearance of the white disc) of the target. As a comparison, fig. 6(f) presents reconstructions obtained from filtered back projection (FBP) and total variation (TV) [26, 33, 12, 32, 13]. Here, data is a concatenation of the 10 gated data sets, thereby corresponding then sampling the ray transform using 100 angles in $[0, \pi]$. Note that the temporal evolution of the target is not accounted for in these reconstructions.

6 Conclusions and discussion

We have introduced a metamorphosis-based framework for indirect registration and showed that this corresponds to a well-defined regularisation method. We also present several numerical examples from tomography supporting this theoretical result.

In particular, section 5.6 illustrates that this framework can be used to recover the temporal evolution of a template from time series data, even when data at each time point is very incomplete. This approach does however assume access to an initial template. In spatio-temporal reconstruction, such an initial template is unknown and it needs to be recovered as well. One approach for doing this is by an intertwined scheme that alternates between to steps (similarly to [21]): (i) given a template, estimate its evolution that is consistent with times series of data using the metamorphosis framework for indirect registration, and (ii) estimate the initial template from times series of data given its evolution. The method in section 5.6 solves the first of the above steps, which is the more difficult one.

Another topic is the choice of hyper-parameters. Our metamorphosis-based framework for indirect registration relies on three parameters with the kernel-size σ being the most important as shown in section 5.5. This parameter has a strong influence on the way the reconstructed image trajectory decomposes into a deformation and a template part. Clearly it acts as a regularisation parameter and a natural problem is to devise a scheme for choosing it bearing in mind the size (scale) of the features undergoing deformation. Unfortunately, similarly to direct registration by LDDMM, the choice of this parameter (and more generally choice of kernel for the RKHS V) is still an open problem [3, 11, 14]. One way is to use a multi-scale approach [8, 30, 34] but a general method for selecting an appropriate kernel-size remains to be determined.

7 Acknowledgements

The work by Ozan ´Oktem, Barbara Gris and Chong Chen was supported by the Swedish Foundation for Strategic Research grant AM13-0049.

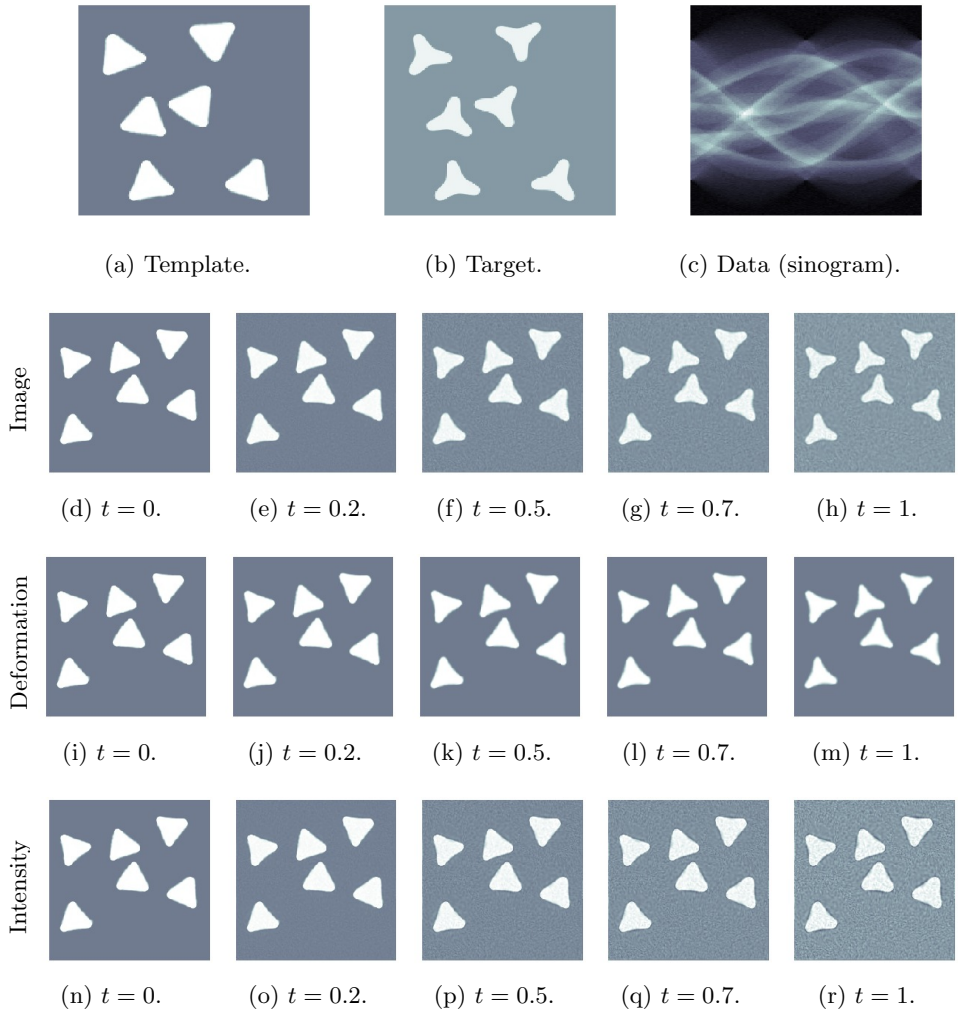

(a) Template. (b) Target. (c) Data (sinogram).

(d) $t = 0$. (e) $t = 0.2$. (f) $t = 0.5$. (g) $t = 0.7$. (h) $t = 1$.

(i) $t = 0$. (j) $t = 0.2$. (k) $t = 0.5$. (l) $t = 0.7$. (m) $t = 1$.

(n) $t = 0$. (o) $t = 0.2$. (p) $t = 0.5$. (q) $t = 0.7$. (r) $t = 1$.

Figure 2: Metamorphosis based indirect-matching of template in (a) against data in (c), which represents 2D ray transform of target in (b) (100 uniformly distributed angles in $[0, \pi]$). The second row (d)–(h) shows the image trajectory $t \mapsto \mathcal{W}(\varphi^{\boldsymbol{\nu}}_{0,t}, f_t(\boldsymbol{\nu}, \zeta))$, so the final registered template is in (h). The third row (i)–(m) shows the deformation trajectory $t \mapsto \mathcal{W}(\varphi^{\boldsymbol{\nu}}_{0,t}, I_0)$, likewise the fourth row (n)–(r) shows the intensity trajectory $t \mapsto f_t(\boldsymbol{\nu}, \zeta)$.

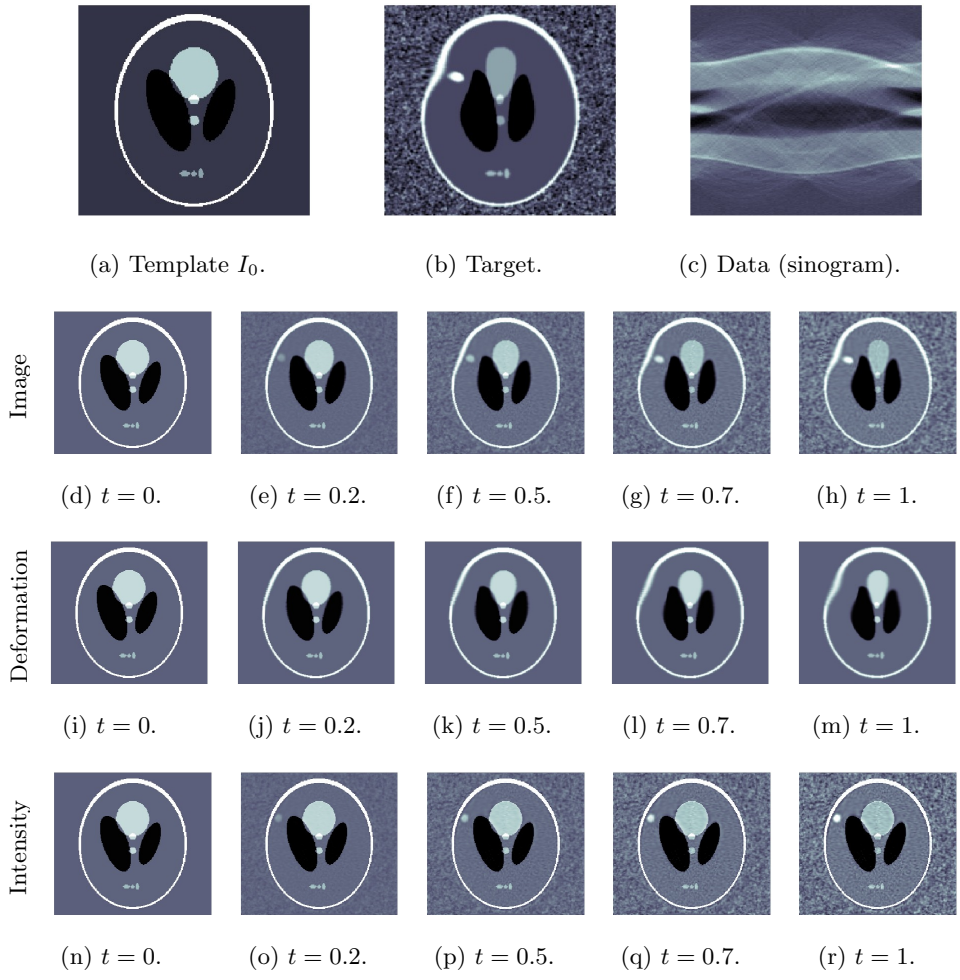

(a) Template I_0. (b) Target. (c) Data (sinogram).

(d) $t = 0$. (e) $t = 0.2$. (f) $t = 0.5$. (g) $t = 0.7$. (h) $t = 1$.

(i) $t = 0$. (j) $t = 0.2$. (k) $t = 0.5$. (l) $t = 0.7$. (m) $t = 1$.

(n) $t = 0$. (o) $t = 0.2$. (p) $t = 0.5$. (q) $t = 0.7$. (r) $t = 1$.

Figure 3: Metamorphosis based indirect-matching of template in (a) against data in (c), which represents 2D ray transform of target in (b) (100 uniformly distributed angles in $[0, \pi]$). The second row (d)–(h) shows the image trajectory $t \mapsto \mathcal{W}(\varphi^{\boldsymbol{\nu}}_{0,t}, f_t(\boldsymbol{\nu}, \zeta))$, so the final registered template is in (h). The third row (i)–(m) shows the deformation trajectory $t \mapsto \mathcal{W}(\varphi^{\boldsymbol{\nu}}_{0,t}, I_0)$, likewise the fourth row (n)–(r) shows the intensity trajectory $t \mapsto f_t(\boldsymbol{\nu}, \zeta)$.

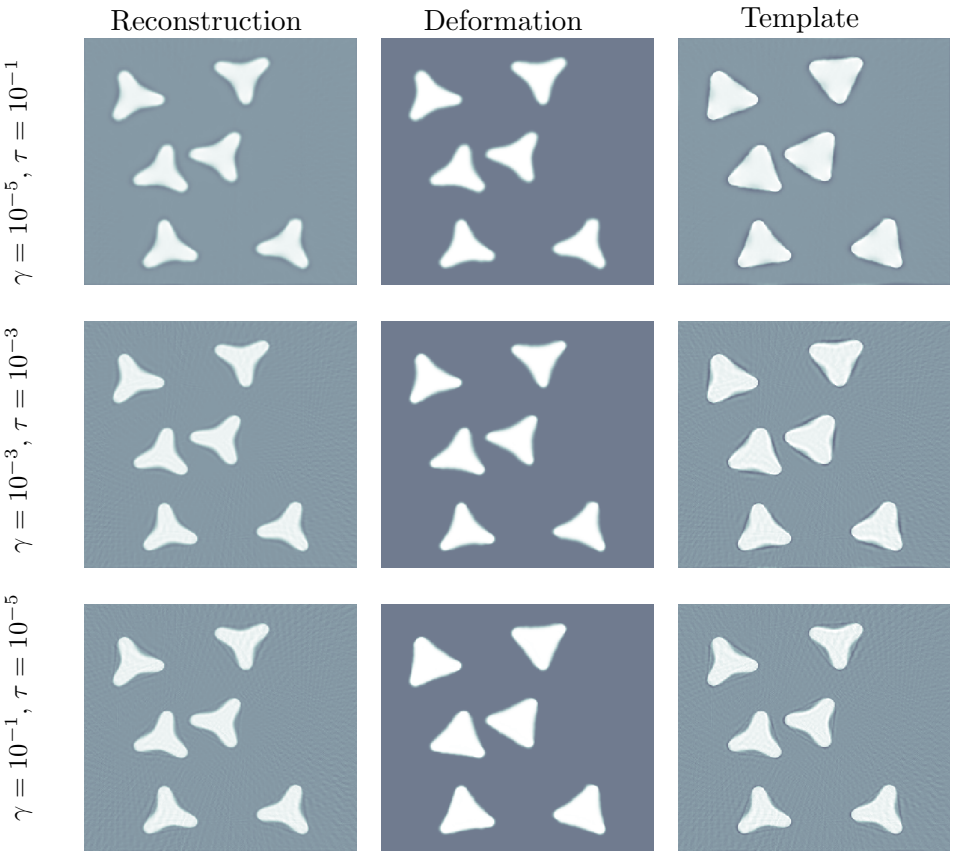

Figure 4: Reconstruction results and their decomposition into template part and deformation part for various regularisation parameters γ and τ.

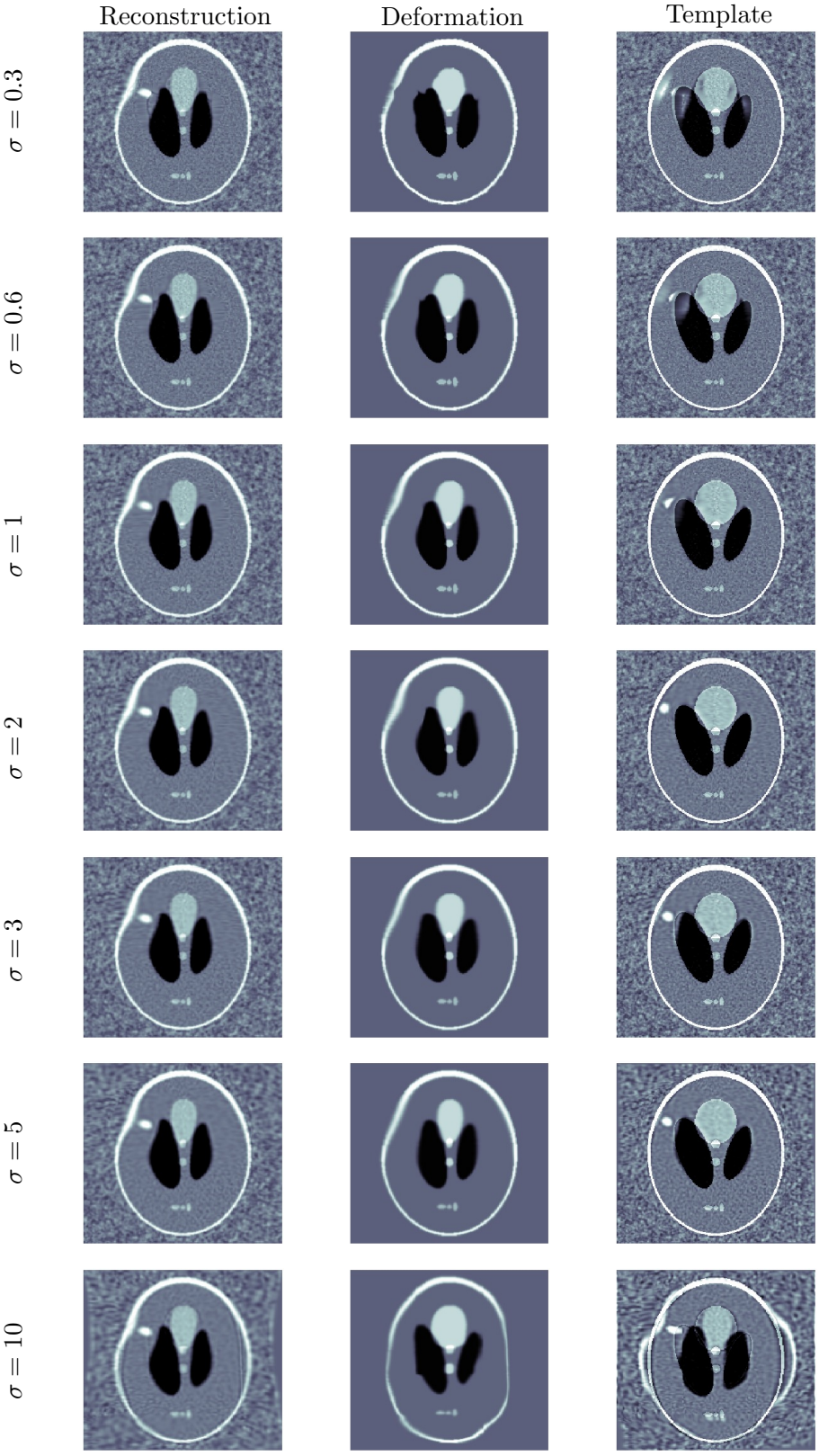

Figure 5: Reconstruction results and their decomposition into template part and deformation part for various kernel size σ. As comparison, the image domain has size 32 in this example.

(a) The temporal evolution of the target.

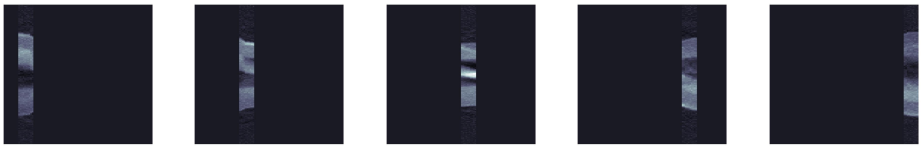

(b) The (gated) tomographic data. Each data set is highly incomplete (limited angle).

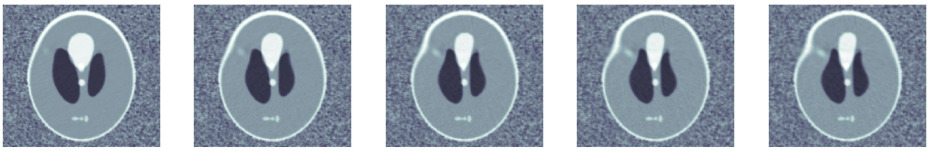

(c) Image trajectory (reconstruction), combines deformation and template trajectories.

(d) Deformation trajectory, models mainly geometric changes.

(e) Template trajectory, models mainly intensity changes.

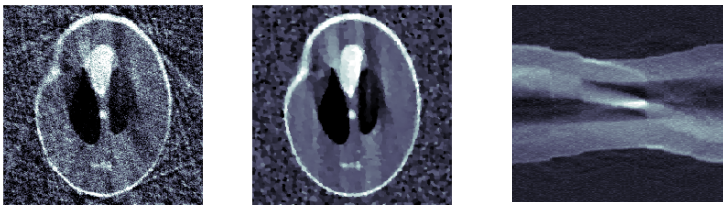

(f) FBP (left) and TV (middle) reconstructions from concatenated data (right).

Figure 6: Reconstructing the temporal evolution of a template using metamorphosis. Target (a), data (b), and results (c)–(e), are shown at selected time points $t = 0.2, 0.4, 0.6, 0.8$, and 1.0. As a comparison we show reconstructions assuming static target obtained from concatenating the gated tomographic data (f).

A Gradient computation

This section presents the computation of the gradient of $\mathcal{J}_{\gamma,\tau}(\,\cdot\,; g)$, which is useful for any first order optimisation metod for minimising the functional $\mathcal{J}_{\gamma,\tau}(\,\cdot\,; g)$ in (8). The computations assume $X = L^2(\Omega, \mathbb{R})$ with

$$I_0 \in X \cap C^1(\Omega, \mathbb{R}) \quad \text{and} \quad (\boldsymbol{\nu}, \zeta) \in L^2\left([0,1], V \times X\right).$$

Furthermore, for each $t \in [0,1]$ we also assume $t \mapsto \zeta(t,\,\cdot\,) \in C^1(\Omega, \mathbb{R})$. In numerical implementations, we consider digitised images and considerations of the above type are not that restrictive.

Let us first compute the differential of the data discrepancy term with respect to ζ using the notation $f_t^{\boldsymbol{\nu},\zeta} := \mathcal{W}(\varphi_{t,0}^{\boldsymbol{\nu}}, I_t^{\boldsymbol{\nu},\zeta}) = I_t^{\boldsymbol{\nu},\zeta} \circ \varphi_{t,0}^{\boldsymbol{\nu}}$. As noted in (14), we have

$$f_t^{\boldsymbol{\nu},\zeta}(x) = (I_t^{\boldsymbol{\nu},\zeta} \circ \varphi_{t,0}^{\boldsymbol{\nu}})(x) = I_0\big(\varphi_{t,0}^{\boldsymbol{\nu}}(x)\big) + \int_0^t \zeta\big(\tau, \varphi_{t,\tau}^{\boldsymbol{\nu}}(x)\big)\mathrm{d}\tau. \tag{28}$$

Then

$$\begin{aligned}
\partial_\zeta\Big[\mathcal{L}\big(f_t^{\boldsymbol{\nu},\zeta}, g\big)\Big](\zeta)(\eta) &= \Big\langle \nabla\,\mathcal{L}(f_t^{\boldsymbol{\nu},\zeta}, g), \partial_\zeta f_t^{\boldsymbol{\nu},\zeta}(\zeta)(\eta)\Big\rangle \\
&= \int_\Omega \int_0^t \nabla\,\mathcal{L}\big(f_1^{\boldsymbol{\nu},\zeta}, g\big)\eta(\tau, \varphi_{t,\tau}^{\boldsymbol{\nu}}(x))\mathrm{d}\tau\mathrm{d}x \\
&= \int_\Omega \int_0^1 1_{\tau\le t}|\operatorname{Det}(\mathrm{d}\varphi_{\tau,t}^{\boldsymbol{\nu}}(x))|\nabla\,\mathcal{L}(f_t^{\boldsymbol{\nu},\zeta}, g)(\varphi_{\tau,t}^{\boldsymbol{\nu}}(x))\eta(\tau, x)\mathrm{d}\tau\mathrm{d}x \\
&= \Big\langle 1_{\cdot\le t}|\operatorname{Det}(\mathrm{d}\varphi_{\cdot,t}^{\boldsymbol{\nu}})|\nabla\,\mathcal{L}(f_t^{\boldsymbol{\nu},\zeta}, g))(\varphi_{\cdot,t}^{\boldsymbol{\nu}}), \eta\Big\rangle_{L^2([0,1],L^2(\Omega,\mathbb{R}))}.
\end{aligned}$$

In order to compute the differential of the discrepancy term with respect to $\boldsymbol{\nu}$, we start by computing the differential of $f_1^{\boldsymbol{\nu},\zeta}$ with respect to $\boldsymbol{\nu}$. Hence, let $\boldsymbol{\mu} \in L^2\left([0,1], V\right)$ and $x \in \Omega$. Then

$$\begin{aligned}
\frac{\mathrm{d}}{\mathrm{d}\epsilon} f_t^{\boldsymbol{\nu}+\epsilon\boldsymbol{\mu},\zeta}(x)\Big|_{\epsilon=0} &= \Big\langle \nabla I_0\big(\varphi_{t,0}^{\boldsymbol{\nu}}(x)\big), \frac{\mathrm{d}}{\mathrm{d}\epsilon}\varphi_{t,0}^{\boldsymbol{\nu}+\epsilon\boldsymbol{\mu}}(x)\big|_{\epsilon=0}\Big\rangle \\
&\quad + \int_0^t \Big\langle \nabla\zeta(\tau, \varphi_{t,\tau}^{\boldsymbol{\nu}}(x)), \frac{\mathrm{d}}{\mathrm{d}\epsilon}\varphi_{t,\tau}^{\boldsymbol{\nu}+\epsilon\boldsymbol{\mu}}(x)\big|_{\epsilon=0}\Big\rangle\mathrm{d}\tau \\
&= -\int_0^t \Big\langle \nabla I_0(\varphi_{t,0}^{\boldsymbol{\nu}}(x)), \mathrm{d}\varphi_{s,0}^{\boldsymbol{\nu}}\big(\varphi_{t,s}^{\boldsymbol{\nu}}(x)\big)\Big(\boldsymbol{\mu}\big(s, \varphi_{t,s}^{\boldsymbol{\nu}}(x)\big)\Big)\Big\rangle\mathrm{d}s \\
&\quad \int_0^t \Big\langle \nabla\zeta\big(\tau, \varphi_{t,\tau}^{\boldsymbol{\nu}}(x)\big), \int_t^\tau \mathrm{d}\varphi_{s,\tau}^{\boldsymbol{\nu}}\big(\varphi_{t,s}^{\boldsymbol{\nu}}(x)\big)\Big(\boldsymbol{\mu}\big(s, \varphi_{t,s}^{\boldsymbol{\nu}}(x)\big)\Big)\mathrm{d}s\Big\rangle\mathrm{d}\tau \\
&= -\int_0^t \Big\langle \nabla I_0\big(\varphi_{t,0}^{\boldsymbol{\nu}}(x)\big), \mathrm{d}\varphi_{s,0}^{\boldsymbol{\nu}}\big(\varphi_{t,s}^{\boldsymbol{\nu}}(x)\big)\Big(\big(\boldsymbol{\mu}\big((s, \varphi_{t,s}^{\boldsymbol{\nu}}(x)\big)\big)\Big)\Big\rangle\mathrm{d}s \\
&\quad -\int_0^t \int_0^s \Big\langle \nabla\zeta(\tau,\,\cdot\,)\circ\varphi_{t,\tau}^{\boldsymbol{\nu}}(x), \mathrm{d}\varphi_{s,\tau}^{\boldsymbol{\nu}}\big(\varphi_{t,s}^{\boldsymbol{\nu}}(x)\big)\Big(\boldsymbol{\mu}\big(s, \varphi_{t,s}^{\boldsymbol{\nu}}(x)\big)\Big)\Big\rangle\mathrm{d}\tau\mathrm{d}s.
\end{aligned} \tag{29}$$

Using (29), we can compute the derivative of $\epsilon \mapsto \mathcal{L}\big(\mathcal{W}(\varphi_t^{\boldsymbol{\nu}+\epsilon\boldsymbol{\mu}}, I_t^{\boldsymbol{\nu}+\epsilon\boldsymbol{\mu},\zeta})\big)$ at $\epsilon = 0$:

$$
\begin{aligned}
\frac{\mathrm{d}}{\mathrm{d}\epsilon}\mathcal{L}\big(\mathcal{W}\big(\varphi_t^{\boldsymbol{\nu}+\epsilon\boldsymbol{\mu}}, I_t^{\boldsymbol{\nu}+\epsilon\boldsymbol{\mu},\zeta}\big)\big)\big|_{\epsilon=0} &= \Big\langle \nabla\,\mathcal{L}\big(f_t^{\boldsymbol{\nu},\zeta}, g\big), \frac{\mathrm{d}}{\mathrm{d}\epsilon} f_t^{\boldsymbol{\nu}+\epsilon\boldsymbol{\mu},\zeta}\big|_{\epsilon=0}\Big\rangle \\
&= -\int_\Omega \Bigg\{ \int_0^t \nabla\,\mathcal{L}\big(f_t^{\boldsymbol{\nu},\zeta}, g\big)(x) \cdot \Bigg[\Big\langle \nabla I_0\big(\varphi_{t,0}^{\boldsymbol{\nu}}(x)\big), \mathrm{d}\varphi_{s,0}^{\boldsymbol{\nu}}\big(\varphi_{t,s}^{\boldsymbol{\nu}}(x)\big)\big(\boldsymbol{\mu}(s, \varphi_{t,s}^{\boldsymbol{\nu}}(x))\big)\Big\rangle \\
&\quad + \int_0^s \Big\langle \nabla\zeta(\tau, \cdot)\circ\varphi_{t,\tau}^{\boldsymbol{\nu}}(x), \mathrm{d}\varphi_{s,\tau}^{\boldsymbol{\nu}}\big(\varphi_{t,s}^{\boldsymbol{\nu}}(x)\big)\Big(\boldsymbol{\mu}\big(s, \varphi_{t,s}^{\boldsymbol{\nu}}(x)\big)\Big)\Big\rangle \mathrm{d}\tau \Bigg] \mathrm{d}s \Bigg\} \mathrm{d}x \\
&= -\int_\Omega \Bigg\{ \int_0^t \Big|\mathrm{Det}\big(\mathrm{d}\varphi_{s,t}^{\boldsymbol{\nu}}(x)\big)\Big| \nabla\,\mathcal{L}\big(f_t^{\boldsymbol{\nu},\zeta}, g\big)\big(\varphi_{s,t}^{\boldsymbol{\nu}}(x)\big) \cdot \\
&\qquad \Bigg[\Big\langle \nabla I_0\big(\varphi_{s,0}^{\boldsymbol{\nu}}(x)\big), \mathrm{d}\varphi_{s,0}^{\boldsymbol{\nu}}(x)\big(\boldsymbol{\mu}(s,x)\big)\Big\rangle \\
&\qquad\quad + \int_0^s \Big\langle \nabla\zeta(\tau, \cdot)\circ\varphi_{s,\tau}^{\boldsymbol{\nu}}(x), \mathrm{d}\varphi_{s,\tau}^{\boldsymbol{\nu}}(x)\big(\boldsymbol{\mu}(s,x)\big)\Big\rangle \mathrm{d}\tau \Bigg] \mathrm{d}s \Bigg\} \mathrm{d}x \\
&= -\int_\Omega \int_0^t \Big|\mathrm{Det}\big(\mathrm{d}\varphi_{s,t}^{\boldsymbol{\nu}}(x)\big)\Big| \nabla\,\mathcal{L}\big(f_t^{\boldsymbol{\nu},\zeta}, g\big)\big(\varphi_{s,t}^{\boldsymbol{\nu}}(x)\big) \cdot \Bigg[\Big\langle \nabla(I_0\circ\varphi_{s,0}^{\boldsymbol{\nu}})(x), \boldsymbol{\mu}(s,x)\Big\rangle \\
&\quad + \int_0^s \Big\langle \nabla(\zeta(\tau, \cdot) \circ \varphi_{s,\tau}^{\boldsymbol{\nu}})(x), \boldsymbol{\mu}(s,x)\Big\rangle \mathrm{d}\tau \Bigg] \mathrm{d}s\mathrm{d}x \\
&= -\int_\Omega \int_0^1 \Bigg\langle 1_{s\le t} \Big|\mathrm{Det}\big(\mathrm{d}\varphi_{s,t}^{\boldsymbol{\nu}}(x)\big)\Big| \nabla\,\mathcal{L}\big(f_t^{\boldsymbol{\nu},\zeta}, g\big)\big(\varphi_{s,t}^{\boldsymbol{\nu}}(x)\big) \\
&\quad \Bigg[\nabla(I_0 \circ \varphi_{s,0}^{\boldsymbol{\nu}})(x) + \int_0^s \nabla(\zeta(\tau, \cdot) \circ \varphi_{s,\tau}^{\boldsymbol{\nu}})(x)\mathrm{d}\tau \Bigg], \boldsymbol{\mu}(s,x)\Bigg\rangle \mathrm{d}s\mathrm{d}x \\
&= -\Bigg\langle 1_{\cdot\le t} \Big|\mathrm{Det}\big(\mathrm{d}\varphi_{\cdot,t}^{\boldsymbol{\nu}}\big)\Big| \nabla\,\mathcal{L}\big(f_t^{\boldsymbol{\nu},\zeta}, g\big) \circ \varphi_{\cdot,t}^{\boldsymbol{\nu}} \\
&\qquad \Bigg[\nabla(I_0\circ\varphi_{\cdot,0}^{\boldsymbol{\nu}})(\,\cdot\,) + \int_0^{\cdot} \nabla(\zeta(\tau, \cdot)\circ\varphi_{\cdot,\tau}^{\boldsymbol{\nu}})(\,\cdot\,)\mathrm{d}\tau \Bigg], \boldsymbol{\mu}\Bigg\rangle_{L^2([0,1],L^2(\Omega,\mathbb{R}^d))} \\
&= -\Bigg\langle \int_\Omega K(x, \cdot) 1_{\cdot\le t} \Big|\mathrm{Det}\big(\mathrm{d}\varphi_{\cdot,t}^{\boldsymbol{\nu}}(x)\big)\Big| \nabla\,\mathcal{L}\big(f_t^{\boldsymbol{\nu},\zeta}, g\big)\big(\varphi_{\cdot,t}^{\boldsymbol{\nu}}(x)\big) \\
&\qquad \Bigg[\nabla(I_0\circ\varphi_{\cdot,0}^{\boldsymbol{\nu}})(x) + \int_0^{\cdot} \nabla(\zeta(\tau, \cdot)\circ\varphi_{\cdot,\tau}^{\boldsymbol{\nu}})(x)\mathrm{d}\tau \Bigg], \boldsymbol{\mu}\Bigg\rangle_{L^2([0,1],V)}.
\end{aligned}
$$

References

[1] S. Arguillere, E. Trélat, A. Trouvé, and L. Younes. Shape deformation analysis from the optimal control viewpoint. *Journal de Mathématiques Pures et Appliqués*, 104(1):139–178, 2015.

[2] M. Bauer, M. Bruveris, and P. W. Michor. Overview of the geometries of shape spaces and diffeomorphism groups. *Journal of Mathematical Imaging and Vision*, 50(1–2):60–97, 2014.

[3] M. F. Beg, M. I. Miller, A. Trouvé, and L. Younes. Computing large deformation metric mappings via geodesic flows of diffeomorphisms. *International journal of computer vision*, 61(2):139–157, 2005.

[4] M. Bertero, H. Lantéri, and L. Zanni. Iterative image reconstruction: a point of view. In Y. Censor, M. Jiang, and A. K. Louis, editors, *Proceedings of the Interdisciplinary Workshop on Mathematical Methods in Biomedical Imaging and Intensity-Modulated Radiation (IMRT), Pisa, Italy*, pages 37–63, 2008.

[5] E. Bladt, D. M. Pelt, S. Bals, and K. J. Batenburg. Electron tomography based on highly limited data using a neural network reconstruction technique. *Ultramicroscopy*, 158:81–88, 2015.

[6] L. G. Brown. A survey of image registration techniques. *ACM computing surveys (CSUR)*, 24(4):325–376, 1992.

[7] M. Bruveris and D. D. Holm. Geometry of image registration: The diffeomorphism group and momentum maps. In D. E. Chang, D. D. Holm, G. Patrick, and T. Ratiu, editors, *Geometry, Mechanics, and Dynamics*, pages 19–56. Springer, 2015.

[8] M. Bruveris, L. Risser, and F.-X. Vialard. Mixture of kernels and iterated semidirect product of diffeomorphisms groups. *Multiscale Modeling & Simulation*, 10(4):1344–1368, 2012.

[9] N. Charon, B. Charlier, and A. Trouvé. Metamorphoses of functional shapes in Sobolev spaces. *Foundations of Computational Mathematics*, pages 1–62, 2016.

[10] C. Chen, B. Gris, and O. Öktem. A new variational model for joint image reconstruction and motion estimation in spatiotemporal imaging. *arXiv preprint*, arXiv:1812.03446, 2018.

[11] C. Chen and O. Öktem. Indirect image registration with large diffeomorphic deformations. *SIAM Journal of Imaging Sciences*, 11(1):575–617, 2018.

[12] C. Chen and G. Xu. Gradient-flow-based semi-implicit finite-element method and its convergence analysis for image reconstruction. *Inverse Problems*, 28(3):035006, 2012.

[13] C. Chen and G. Xu. A new linearized split Bregman iterative algorithm for image reconstruction in sparse-view X-ray computed tomography. *Comput. Math. Appl.*, 71(8):1537–1559, 2016.

[14] S. Durrleman, M. Prastawa, N. Charon, J. R. Korenberg, S. Joshi, G. Gerig, and A. Trouvé. Morphometry of anatomical shape complexes with dense deformations and sparse parameters. *NeuroImage*, 101:35–49, 2014.

[15] A. Effland, M. Rumpf, and F. Schäfer. Image extrapolation for the time discrete metamorphosis model: Existence and applications. *SIAM Journal of Imaging Sciences*, 11(1):834–862, 2018.

[16] F. Gigengack, L. Ruthotto, M. Burger, C. H. Wolters, X. Jiang, and K. Schäfers. Motion correction of cardiac pet using mass-preserving registration. In *IEEE Nuclear Science Symposuim & Medical Imaging Conference*, pages 3317–3319. IEEE, 2010.

[17] F. Gigengack, L. Ruthotto, M. Burger, C. H. Wolters, X. Jiang, and K. P. Schäfers. Mass-preserving motion correction of pet: Displacement field vs. spline transformation. In *2011 IEEE Nuclear Science Symposium Conference Record*, pages 3088–3090. IEEE, 2011.

[18] F. Gigengack, L. Ruthotto, M. Burger, C. H. Wolters, X. Jiang, and K. P. Schafers. Motion correction in dual gated cardiac pet using mass-preserving image registration. *IEEE transactions on medical imaging*, 31(3):698–712, 2011.

[19] M. Grasmair. Generalized Bregman distances and convergence rates for non-convex regularization methods. *Inverse Problems*, 26(11):115014, 2010.

[20] G. T. Gullberg, B. W. Reutter, A. Sitek, J. S. Maltz, and T. F. Budinger. Dynamic single photon emission computed tomography – basic principles and cardiac applications. *Physics in Medicine and Biology*, 55:R111–R191, 2010.

[21] J. Hinkle, M. Szegedi, B. Wang, B. Salter, and S. Joshi. 4D CT image reconstruction with diffeomorphic motion model. *Medical image analysis*, 16(6):1307–1316, 2012.

[22] A. Mang and G. Biros. Constrained Hˆ1-regularization schemes for diffeomorphic image registration. *SIAM journal on imaging sciences*, 9(3):1154–1194, 2016.

[23] A. Mang and L. Ruthotto. A Lagrangian Gauss–Newton–Krylov solver for mass-and intensity-preserving diffeomorphic image registration. *SIAM Journal on Scientific Computing*, 39(5):B860–B885, 2017.

[24] A. Markoe. *Analytic Tomography*, volume 106 of *Encyclopedia of mathematics and its applications*. Cambridge University Press, 2006.

[25] M. I. Miller, L. Younes, and A. Trouvé. Diffeomorphometry and geodesic positioning systems for human anatomy. *Technology*, 2(1), 2014.

[26] F. Natterer. *The Mathematics of Computerized Tomography*, volume 32 of *Classics in Applied Mathematics*. SIAM, 2001.

[27] F. Natterer and F. Wübbeling. *Mathematical Methods in Image Reconstruction*. Mathematical Modeling and Computation. Society for Industrial and Applied Mathematics, 2001.

[28] S. Neumayer, J. Persch, and G. Steidl. Regularization of inverse problems via time discrete geodesics in image spaces. *Inverse Problems*, 35(5):055005, 2019.

[29] O. Öktem, C. Chen, N. O. Domaniç, P. Ravikumar, and C. Bajaj. Shape based image reconstruction using linearised deformations. *Inverse Problems*, 33(3):035004, 2017.

[30] L. Risser, F.-X. Vialard, R. Wolz, M. Murgasova, D. D. Holm, and D. Rueckert. Simultaneous multi-scale registration using large deformation diffeomorphic metric mapping. *IEEE transactions on medical imaging*, 30(10):1746–1759, 2011.

[31] A. Schwarz and M. Leach. Implications of respiratory motion for the quantification of 2D MR spectroscopic imaging data in the abdomen. *Physics in Medicine and Biology*, 45(8):2105—2116, 2000.

[32] E. Sidky, J. Jørgensen, and X. Pan. Convex optimization problem prototyping for image reconstruction in computed tomography with the Chambolle–Pock algorithm. *Physics in medicine and biology*, 57(10):3065, 2012.

[33] E. Sidky, C. Kao, and X. Pan. Accurate image reconstruction from few-views and limited-angle data in divergent-beam CT. *Journal of X-ray Science and Technology*, 14(2):119–139, 2006.

[34] S. Sommer, M. Nielsen, F. Lauze, and X. Pennec. A multi-scale kernel bundle for LDDMM: towards sparse deformation description across space and scales. In *Biennial International Conference on Information Processing in Medical Imaging*, pages 624–635. Springer Verlag, 2011.

[35] A. Sotiras, C. Davatzikos, and N. Paragios. Deformable medical image registration: A survey. *IEEE Transactions on Medical Imaging*, 32(7):1153–1190, 2013.

[36] A. Trouvé and L. Younes. Metamorphoses through Lie group action. *Foundations of Computational Mathematics*, 5(2):173–198, 2005.

[37] Y. Wang, E. Vidan, and G. Bergman. Cardiac motion of coronary arteries: Variability in the rest period and implications for coronary MR angiography. *Radiology*, 213(3):751—758, 1999.

[38] Z. Wang, A. C. Bovik, H. R. Sheikh, and E. P. Simoncelli. Image quality assessment: From error visibility to structural similarity. *IEEE Trans. Image Process.*, 13:600–612, 2004.

[39] A. Wirgin. The inverse crime. *ArXiv preprint*, 0401050, 2004.

[40] L. Younes. *Shapes and Diffeomorphisms*, volume 171 of *Applied Mathematical Sciences*. Springer-Verlag, 2010.

[41] B. Zitova and J. Flusser. Image registration methods: a survey. *Image and vision computing*, 21(11):977–1000, 2003.